Drugs in a curative combination therapy for lymphoma exhibit low cross-resistance but not pharmacological synergy

Adam C Palmer[1*], Christopher Chidley[1*], and Peter K Sorger[1,2]

[1] Laboratory of Systems Pharmacology
[2] Department of Systems Biology
Harvard Medical School
200 Longwood Avenue
Boston MA 02115

*These authors contributed equally.

† Pre-publication correspondence should be addressed to Peter Sorger (peter_sorger@hms.harvard.edu); copying Chris Bird (617-432-6901/6902).

Peter K Sorger: orcid.org/0000-0002-3364-1838

The authors have no competing interests.

SUMMARY

Almost all curative cancer therapies involve multi-drug combinations. The development of new combinations currently focuses on identifying instances of synergistic pharmacological interaction. Historically successful curative therapies were developed by experimentation in humans using different criteria but the mechanistic basis of these successful combinations has not been investigated in detail. Here we use isobologram analysis to score pharmacological interaction and clone-tracing and CRISPR screening to measure cross-resistance among the five drugs comprising R-CHOP, a combination therapy that frequently cures Diffuse Large B-Cell Lymphomas. We find that drugs in R-CHOP exhibit very low cross-resistance but no synergy; their combined activity is close to dose-additive (Loewe model) and effect-independent (Bliss model). These data provide direct evidence for the 50-year old hypothesis that a curative cancer therapy can be constructed on the basis of non-overlapping resistance among individually effective drugs, rather than pharmacological interaction.

SIGNIFICANCE

The use of combinations of anti-cancer drugs is widely regarded as essential for improving rates of therapeutic response and minimizing acquired resistance. The design of new combinations usually begins with pre-clinical studies involving dose response landscapes and a search for combinations that exceed the expectations of Loewe Additivity or Bliss Independence, and therefore score as synergistic. Our data show that a highly successful combination therapy achieving the very high bar of curing Diffuse Large B-Cell Lymphomas works due to low cross-resistance among drugs, not synergy. Low cross-resistance allows highly efficient killing of heterogeneous populations of cancer cells. This insight has immediate significance for the design of new drug combinations by prioritizing measurement of cross-resistance and individual drug potency, and deemphasizing synergy as a litmus-test. New barcoding and CRISPR technology make such cross-resistance screens feasible.

INTRODUCTION

The majority of cancers are treated with combination therapies. For some types of cancer, multidrug combinations produce frequent cures, whereas cure by monotherapy is rare (1). In current practice, the search for new drug combinations focuses on identifying drugs that exhibit synergy. Although "synergy" can be used loosely it is best defined by Bliss or Loewe criteria, which test whether a combination is stronger than expected from the sum of the drugs' individual effects (2-5); antagonism arises when combinations are less active than additivity would predict. In translational cancer biology such measurements are most commonly made using cultured cells or genetically defined mouse models. Despite the current emphasis on synergy, historically successful combinations were developed according to quite different hypotheses. For example, Law (6, 7) and Frei*, et al.* (8) argued for combining drugs having non-overlapping mechanisms of resistance that might be expected to overcome clonal heterogeneity present within each patient's cancer. Heterogeneity between patients can also be a reason why drug combinations improve response rates, even if each patient only benefits from the most active monotherapy (9). However, because monotherapies are almost never curative, curative drug combinations must undoubtedly surpass the most active monotherapy, and thus cannot be explained by patient variability. The mixtures of drugs making up curative regimens were generally developed based on empirical experimentation in patients and such combinations have only rarely been subjected to detailed mechanistic analysis.

Testing whether a drug combination exhibits synergy can be accomplished *ex vivo* by measuring and analyzing the responses of cells to drugs applied individually and in combination over a range of concentrations, for example by isobologram analysis (4, 10). Testing whether a combination exhibits low cross-resistance is more challenging because it requires systematic exploration of resistance mechanisms (different mechanisms of resistance display different cross-resistance properties). It has long been possible to isolate cell clones resistant to single drugs and then assay for sensitivity to other

drugs, but this approach is not practical at a scale needed to test Law and Frei's hypothesis, as was recognized by Law (7). Efficient analysis of cross-resistance has become feasible only recently with technical breakthroughs in multiplexed clone tracing and reverse genetic screening. DNA barcode libraries allow large numbers ($\geq 10^6$) of uniquely tagged clones to be tested in parallel for resistance to multiple drugs (11), and genetic screens using CRISPR-Cas9 systems or Open Reading Frame libraries enable genome-wide identification of loss and gain of function changes that confer resistance (12-18). To date, barcode and CRISPR-Cas9 libraries have been used to study mechanisms of resistance primarily to targeted therapies and identify novel combinations of such drugs (11, 19); they have not yet been used to analyze combinations of cytotoxic drugs that are the backbone of curative therapies and thereby test Law and Frei's 'non-overlapping resistance' hypothesis.

In this paper we measure pharmacological interaction and cross-resistance among components of R-CHOP, a five drug chemo-immunotherapy that achieves high cure rates in Diffuse Large B-Cell Lymphoma (DLBCL). R-CHOP is composed of five constituents: R – rituximab, a humanized monoclonal antibody against CD20, a protein expressed on the surface of all B cells; C – cyclophosphamide (Cytoxan® or Neosar®) an alkylating agent; H – hydroxydaunomycin (doxorubicin, Adriamycin® or Rubex®), a topoisomerase II inhibitor; O – Oncovin® (vincristine), an anti-microtubule drug and; P – prednisone, a steroid. R-CHOP was developed over an extended period of time via clinical experiments in humans (20). The constituent of R-CHOP are known to be individually active on DLBCL cells *in vivo*, and the drugs have largely non-overlapping dose-limiting toxicities, which permits their combined administration in patients. However the pharmacological principles underlying the clinical superiority of R-CHOP in DLBCL remain poorly understood. The key question for contemporary drug discovery is which among several different properties of a combination should be given the greatest weight: low cross-resistance as previously proposed, or pharmacological interaction and synergy as currently emphasized (21, 22).

We tested for pharmacological interaction among all pairs of R-CHOP constituents across a full dose range in three cell lines and assessed interaction using both the Bliss independence and Loewe additivity criteria. We observed little if any synergy: most drug pairs were additive and some were antagonistic. We also tested higher order combinations at fixed dose ratios with similar results. We screened for cross resistant mutations using random mutagenesis with clone tracing, and both CRISPR interference (CRISPRi) and CRISPR activation (CRISPRa) screening. The rate of multi-drug resistance was near the theoretical minimum predicted by Law (6), suggesting that low cross-resistance is a key attribute of the curative R-CHOP regimen.

RESULTS

Components of R-CHOP do not exhibit synergy in killing Diffuse Large B-Cell Lymphoma cells

Pharmacological interactions among R-CHOP constituents were measured in human Pfeiffer, SU-DHL-4 and SU-DHL-6 cell lines. All three lines are derived from germinal center B-like DLBCL (23), the subtype most responsive to R-CHOP (24). Prednisone and cyclophosphamide are pro-drugs that are activated by liver metabolism. We therefore used the pre-activated forms of these drugs: prednisolone and 4-hydroperoxy-cyclophosphamide (which spontaneously converts to the active compound 4-hydroxy-cyclophosphamide in water) (25, 26). Rituximab kills B-cell lymphomas through multiple CD20-dependent mechanisms that include complement-mediated cytotoxicity, antibody-dependent cell cytotoxicity (ADCC) and direct killing via CD20 cross-linking (27). Rituximab can kill DLBCL cells in culture via complement-mediated cytotoxicity when human serum is included in the culture media (28). In our hands the cytotoxicity of rituximab to DLBCL cultures was strongly enhanced by human serum (Supplementary Figure 1a). Among seven DLBCL cell lines tested, none exhibited a cytotoxic response to prednisolone alone at clinically relevant concentrations (29), although the rate of cell division was reduced (Supplementary Figure 1b). Prednisone is cytotoxic to DLBCL in first-line

clinical care (30); the absence of cytotoxicity in DLBCL cell culture, consistent with other studies (31), might reflect selection for complete prednisone resistance in cell lines established from post-treatment patients. As there exist no commercially available treatment-naïve DLBCL cell lines, we are not able to test whether such cultures might respond *in vitro* to prednisone/prednisolone.

Pharmacodynamic interactions among drugs comprising R-CHOP were first measured in Pfeiffer cells. For each of 10 drug pairs an 11×11 'checkerboard' was created with each drug increasing in concentration along one of the two axes, spanning a 100-fold range. Cells were incubated with drugs for 72 hours, which by comparison to human pharmacokinetics, spans at least one *in vivo* half-life for each of C, H, O and P (32-34); R has an elimination half-life of 3 weeks in humans (35). Cell viability was measured using a luminescent ATP assay (Cell TiterGlo) that was linearly proportional to live cell number as determined by microscopy and trypan blue vital stain (Supplementary Figure 1c). The ratio of cell number in drug-treated and untreated control cultures (relative cell number) was used to compute normalized growth rate inhibition values (GR values (36)) (Supplementary Figure 1d). Pharmacological interaction was then assessed based on excess over Bliss Independence and by isobologram analysis (which tests for Loewe additivity (5)). We have previously used isobologram analysis to confirm synergistic interaction among HER2 and CDK4/6 inhibitors in breast cancers, which serves as a positive control for the identification of synergy by drug-drug 'checkerboard' experiments (37).

In the Bliss model, drugs are scored as interacting only if their combined effect exceeds a null model of independence involving statistically independent probabilities of cell killing; independence arises when relative (viable) cell numbers for a specific dose of each drug can be multiplied to obtain the cell number for the combination (this is equivalent to adding the log-transformed killing ratios or 'log-kills') (3). By this analysis, we find that pairs of drugs in R-CHOP are largely independent, except that killing by O is strongly antagonized by the presence of either C or H (Figure 1a). Antagonism may be a

consequence of the effects of these drugs on the cell cycle: killing of mitotic cells by O is expected to fall when C- or H-induced DNA damage prevents entry into mitosis (38-40).

In isobologram analysis, contour lines (isoboles) corresponding to a constant phenotype (the fraction of cells killed) are plotted across a two-way dose-response landscape (4, 10). As described by Loewe (4), the shape of the contours is diagnostic of drug interaction: straight contours correspond to drug additivity, convex contours to synergy and concave contours to antagonism (Figure 1b, inset). Isobologram analysis of drug pairs in R-CHOP confirmed results from Bliss analysis, namely that interactions among R-CHOP constituents range from strongly antagonistic to approximately additive (Figure 1b). As discussed earlier, prednisolone was not cytotoxic on its own but it slightly sensitized cells to C and to H. Moreover, complement mediated cytotoxicity by rituximab was approximately additive with each of C, H, and O. As was observed using the Bliss method of analyzing drug interaction, C and H severely antagonized O. Overall, no drug pair showed a beneficial effect exceeding 2-fold deviation from additivity, the minimal recommended threshold for avoiding false-positive claims of synergy (41).

To test for higher-order interactions among all five drugs, we measured viable cell number following exposure of each of three different DLBCL cell lines to all 26 possible combinations of 2, 3, 4, or 5 drugs (Figure 2a). Because high order combinations cannot feasibly be studied across multi-dimensional dose 'checkerboards', R-CHOP constituents were tested at fixed ratios scaled so that constituents were equipotent with respect to cell killing when assayed individually (Supplementary Figure 2a). The activity of drug combinations was then quantified by *Fractional Inhibitory Concentrations* (FIC (42), also known as *Combination Index* (43)), which is a fixed-ratio simplification of Loewe's isobologram analysis (additive contours have FIC=1 by definition). In all three DLBCL cells, we observed that small excesses over additivity for R and P on CHO was balanced by antagonism within CHO, producing net effects ranging from approximately additive to antagonistic (for 5-drugs in

Pfeiffer FIC = 0.8±0.15; for SU-DHL-6 FIC = 1.1±0.3 and for SU-DHL-4 FIC = 1.7±0.2; 95% confidence, n=4-8; Figure 2b, c). The absence of synergy across high order combinations was supported by Bliss analysis of the same data (Supplementary Figure 2b). Emergent pharmacological interactions involving combinations of 3 or more drugs can be identified as deviations from the assumption of dose additivity using data from lower-order drug interactions (44); nearly all such terms supported the hypothesis of no interaction (emergent FIC=1) with the only substantial deviations representing antagonism (emergent FIC=1.5) (Supplementary Figure 2c). We conclude that R-CHOP does not exhibit significant synergy among its constituent drugs.

DLBCL clones resistant to one drug in R-CHOP rarely resist multiple drugs

To test the hypothesis that low cross-resistance is important for a curative therapy we asked whether clones resistant to any single drug in R-CHOP remain susceptible to at least one other drug in the combination. DLBCL genomes are relatively complex, possessing a mixture of single nucleotide polymorphisms and copy number gains and losses (45, 46), and we therefore looked for resistance mutations using three complementary approaches: (i) random mutagenesis coupled to clone tracing, (ii) genetic knockdown via genome-wide CRISPR interference (CRISPRi) for loss of function mutations, and (iii) overexpression via genome-wide CRISPR activation (CRISPRa) for gain of function mutations (Figure 3a). In a hypothetical multi-drug treatment, it is not possible to distinguish between single-drug or multi-drug resistance as either could increase the survival of a mutated clone (Figure 3b). A further complication is that strongly antagonistic drug combinations, such as C, H, and O, can select for *sensitivity* to the antagonizing agent (47). We therefore scored mutations as conferring true cross-resistance by applying drugs individually and identifying those barcodes that were significantly enriched in two or more conditions (Figure 3c). This was accomplished by generating a pool of mutagenized/CRISPR-transformed cells in which each cell carried a unique DNA barcode (or single

guide RNA that also acts as a barcode). Cells were split into independent cultures and then treated with a single R-CHOP component. The abundance of DNA barcodes in each culture was measured before and after drug exposure by next-generation DNA sequencing followed by enrichment analysis.

For random mutagenesis and clone tracing, Pfeiffer cells were mutagenized with N-ethyl-N-nitrosourea (ENU), which induces point mutations and chromosome aberrations (48, 49). One million mutagenized clones were barcoded using a lentiviral DNA barcode library (ClonTracer, (11)). Due to high library complexity ($\approx 7\times10^7$ barcodes) and infection at low multiplicity (0.1), over 99% of clones are expected to contain a unique barcode. Barcoded cells were expanded in puromycin to select for the lentiviral vector. From a single well-mixed suspension of cells, a batch was reserved to measure pre-treatment barcode frequencies, and the remainder was distributed into 18 replicate cultures (3 per drug tested) with each culture providing 12-fold coverage of barcoded clones (Supplementary Figure 3a).

To model the clinical scenario of strong selection pressure from intensive treatment cycles (as opposed to continuous low dose therapy), drugs were applied for 72 hours at a dose established in a pilot study as the highest dose allowing any surviving cells to re-grow in drug-free media in under 2 weeks (Methods). Cultures were exposed to two rounds of drug treatment followed by a recovery period of 4 to 11 days as needed (Supplementary Figure 3a). Because prednisolone monotherapy only slowed growth, cells were treated with prednisolone at 20 μM for 20 days (the R-CHOP regimen contains multiple five-day courses of prednisone). Following the final recovery period, enrichment for specific clones was calculated based on relative barcode frequencies prior to and after treatment.

Thousands of clones were reproducibly enriched in replicate cultures exposed to the same drug. To score cross-resistance and account for culture-to-culture variation across repeats, we constructed an error model by scrambling barcode identities within each replicate. This revealed that at least 300 times as many barcodes were ≥10-fold enriched in repeat experiments for any single drug than expected by chance (Figure 4a). We also accounted for fitness differences observed in vehicle-only cultures (~1% of

barcodes were enriched ≥ 10-fold in the presence of DMSO; see Methods). Correlations between enrichment scores in replicate drug treatments were highly significant ($p<10^{-900}$; $n\approx 10^6$) although of modest magnitude (rank correlation between 0.1 and 0.3). This arises because drug exposure imposes population bottlenecks on non-resistant clones, which represent the majority of the population, causing barcodes to be detected, or not, on a stochastic basis. Among barcodes for which measurements were available in each of two replicates, correlation was higher (0.35 to 0.58) (Supplementary Figure 4b). We used the geometric mean of enrichment for each barcode as a metric of drug resistance across replicates. Instances of stochastic (and thus irreproducible) enrichment are strongly penalized by this metric; conversely, barcodes are favored if they are reproducibly enriched in independent cultures (which is evidence of heritability).

The error model constructed for scrambled barcodes was used to estimate the false discovery rate for barcode enrichment. We found that the stronger the geometric mean enrichment, the less likely it was for such enrichment to occur by random chance (Figure 4c). False discovery of coincident enrichment exceeding 10-fold in 2 or more drugs was rare (<2.5%) and we therefore selected this threshold for all subsequent analysis. For each of the four individually active drugs (i.e. RCHO), 2,000 to 13,000 barcodes were identified with geometric mean enrichment ≥10-fold, representing resistance frequencies of 2×10^{-3} to 1×10^{-2}. The vast majority of enriched clones were unique to one drug, with only 30 to 300 clones (depending on the pair of drugs) enriched in two different conditions (which is diagnostic of double drug-resistance; Figures 4d and 4e). Triple drug-resistant clones were even less abundant (between 1 and 10 clones per set of three drugs) and no clones were found to confer resistance to R, C, H and O (Figure 4e). Clones enriched by prolonged culture at prednisolone concentrations that slowed growth (but did not kill cells) also exhibited low overlap with barcodes enriched for other constituents of R-CHOP (Supplementary Figure 4).

CRISPRi/a screening identifies diverse mechanisms of drug resistance

Screening genome-wide collections of single guide RNA (sgRNAs) by CRISPR makes it possible to identify and compare genes conferring resistance to different drugs (as opposed to barcodes for unknown ENU-mutated loci). CRISPRi yields loss of function resistance mutations and CRISPRa yields over-expression mutations. CRISPRi screening was performed in Pfeiffer cells expressing nuclease-dead Cas9 fused to the transcriptional repression domain KRAB (dCas9-KRAB) (50). CRISPRa screening was performed in cells co-expressing dCas9 fused to the SunTag and a SunTag-binding antibody fused to the VP64 transcriptional activator (51). This approach to CRISPRa requires clonal selection to generate a starting cell population in which the ratio of dCas9:VP64 is fixed (otherwise screening is compromised by high cell-to-cell variability). We were unable to generate monoclonal lineages of Pfeiffer cells expressing dCas9 and VP64 despite multiple attempts, and in other DLBCL cell lines lentiviral transduction was inefficient (a known property of B lymphocytes and lymphomas (52)). We therefore performed CRISPRa screens in the K562 chronic myeloid leukemia (CML) cell line, which can be efficiently transduced and cloned. For CRISPRi in Pfeiffer cells it was possible to screen for resistance to four drugs (R, C, H and O) but for CRISPRa in K562 cells, screening was possible only for C, H and O (these drug mechanisms have been used historically in the treatment of CML).

We used RT-qPCR to confirm that transduction of sgRNAs in cells expressing the appropriate dCas9 fusion protein caused strong repression of a set of test target genes by CRISPRi (in Pfeiffer cells) and strong activation of the targets by CRISPRa (in K562 cells) (Supplementary Figure 5a). We then used lentivirus at low multiplicity ($\leq$0.4) to infect CRISPRi and CRISPRa-expressing cells with second generation genome-scale sgRNA libraries, which are highly active by virtue of having optimized target sites that account for nucleosome positioning (53). Both libraries contained 10 sgRNAs per gene, and approximately 4000 control sgRNAs designed to have no target. Infected cells were expanded under

puromycin selection and exposed to drug (or vehicle) for two to three 72-hr drug pulses separated by recovery periods of up to 5 days as needed. Next-generation sequencing of sgRNAs was then used to identify hits. The impact of each sgRNA on drug sensitivity was quantified by the 'rho phenotype' (54), which is 1 in the case of complete resistance, 0 in the case of sensitivity matching the parental cell line (as determined using non-targeting control sgRNAs), and <0 for enhanced sensitivity (Methods). Across 10 sgRNAs for each gene we calculated the mean of the strongest 5 rho phenotypes by absolute value, and the *p*-value of all 10 rho phenotypes as compared to 4000 non-targeting sgRNAs (using a Mann-Whitney test) (50). From rho phenotypes of 4000 non-targeting sgRNAs measured in each condition, random permutations of 10 were assembled to create ≈19,000 'negative control genes', matching the number of real gene targets and with phenotypes specific to each drug screen. For all four drugs tested, plots of gene phenotype vs. significance ('volcano plots') revealed many significantly enriched and depleted genes as compared to negative control genes (Figure 5 and Supplementary Data).

Hits from CRISPRi and CRISPRa were consistent with known mechanisms of drug action: knockdown of therapeutic drug targets was observed to confer resistance to rituximab (*MS4A1* encoding CD20) and doxorubicin (*TOP2A* encoding topoisomerase II) (27, 55) whereas overexpression of *TUBB* conferred vincristine resistance; *TUBB* encodes β-tubulin, the primary target of vincristine. Multiple genes involved in DNA damage response were identified by CRISPRi as determining resistance or hypersensitivity to cyclophosphamide. Cyclophosphamide functions by inducing interstrand crosslinks in genomic DNA via alkylation; resistance was conferred by knockdown of *SLFN11*, which alters sensitivity to many DNA damaging agents by blocking progression of stressed replication forks (56, 57). Hypersensitivity to cyclophosphamide (which was best detected in a supplementary screen performed at a lower dose of drug; Supplementary Figure 5b,c), was caused by knockdown of genes involved in DNA interstrand crosslink repair (e.g. *FANCE*, *FANCD2*, *UBE2T*, *FANCI*, *ATRIP*) and double-strand break repair (e.g. *BRIP1*, *BARD1*, *BRCA1*, *BRCA2*). The therapeutic window for cyclophosphamide arises

from differential cellular expression of aldehyde dehydrogenases (ALDH) which are the primary enzymes involved in cyclophosphamide inactivation (58, 59). CRISPRa screens found that strong cyclophosphamide resistance was conferred by overexpression of *ALDH1A1* and *ALDH1B1*, and also by overexpression of several aldo-keto reductases (AKRs) that metabolize cytotoxic products of cyclophosphamide, such as acrolein and aldophosphamide (60). From these data we conclude that CRISPRi/a screening successfully identifies biologically relevant genes involved in resistance to the R-CHOP constituents RCHO. Detailed study of these genes is beyond the scope of the current manuscript but we provide the full results for all seven screens in Supplementary Data.

Knockdown and over-expression mutations identified by CRISPRi/a do not confer pan-drug resistance

Next we asked whether any of the knockdown or overexpression mutants identified by CRISPRi/a confer resistance to multiple drugs. For each screen, we calculated a single resistance score which takes into account both effect size and the significance of enrichment (mean rho phenotype $\times$ -$\log_{10}$P). To assess the rate of false discovery of resistance and cross-resistance, we generated 10 complete sets of ≈19,000 negative control genes (matching the number of real genes targeted) and calculated their resistance scores in each screen. A cutoff was identified for which fewer than one negative control gene per set would be assessed as resistant to two drugs. This avoids false discovery of multi-drug resistance but is more tolerant of false discovery for single-drug resistance than is common. By using a less stringent cutoff we avoid rejecting potential examples of cross-resistance and therefore make the test of the Frei and Law hypothesis *more* stringent (see methods and Supplementary Figure 6a and 6c). From CRISPRi screening data we identified 19 genes whose knockdown conferred resistance to two different drugs, and 4 genes that conferred resistance to three drugs (Figure 6a, 6b and Supplementary Figure 6b). *CAD* and *SMARCE1* are examples of genes for which CRISPRi confers

resistance to rituximab and doxorubicin. *CAD* encodes a protein involved in pyrimidine biosynthesis whose knockdown has been reported to protect cells against the microtubule-depolymerizing drug rigosertib. This likely arises from imposition of an S phase arrest that blocks entry into mitosis, where rigosertib exerts its cytotoxic effects (17). *SMARCE1* is a member of the SWI/SNF chromatin-remodeling complex that plays a tumor suppressor role in a wide variety of cancers, including DLBCL (61). CRISPRi of another SWI/SNF protein (*ARID1A*) also conferred rituximab resistance. The four genes whose knockdown conferred triple drug resistance included components of the mediator complex, translation initiation, chromatin modification, and protein degradation. In each of these cases, the degree of resistance was mild (resistance score < 2) and CRISPRi markedly reduced proliferation in the absence of drug treatment (Supplementary Data). We hypothesize that these loss-of-function mutations perturb general features of proliferating cells needed for chemotherapies to be cytotoxic, as has been reported for *CAD* (which conferred two-drug resistance in our screen) (17). No genes were identified by CRISPRi whose knockdown conferred resistance to RCHO.

Screening by CRISPRa identified 42 genes whose overexpression conferred resistance to two drugs and 4 genes that conferred resistance to three drugs (Figure 6c, 6d and Supplementary Figure 6d). *ABCB1* (multidrug resistance protein 1) and *ABCC1* (multidrug resistance-associated protein 1) are members of the ATP-binding cassette (ABC) transporter family whose over-expression results in resistance to H and O, but not to C (Figure 6c). Overexpression of a third ABC gene, *ABCG2*, conferred resistance to H alone (Figure 5); upregulation of drug export via overexpression of ABC transporters is implicated in resistance to many drugs (62, 63). Two of four genes whose activation conferred triple drug resistance (to C, H and O) were linked to glutathione biosynthesis: *GCLC* (Glutamate-cysteine ligase catalytic subunit), which catalyzes the first step in glutathione production, and *NFE2L2* (nuclear factor erythroid 2-related factor 2), the transcription factor for *GCLC* and other genes involved in responsiveness to xenobiotics and oxidative stress (Figure 6c; (64, 65). Glutathione plays an important

role in resistance to chemotherapy (66), and high expression of members of the glutathione gene family is strongly associated with poor overall survival in DLBCL patients treated with CHOP (67). The rate of glutathione synthesis is limited by the enzymatic activity of GCLC and the abundance of cysteine, which is one of three precursors of glutathione. Further supporting the importance of glutathione for responsiveness to chemotherapy, knockdown of *GCLC* conferred hypersensitivity to H and O, and knockdown of the main transporter of cysteine, *SLC7A11*, conferred hypersensitivity to H (Figure 5). From these data we conclude that a substantial number of genes found by CRISPRa to confer resistance to multiple R-CHOP components are associated with previously described or suspected mechanisms of drug resistance. However, we observe that a majority of mechanisms of 'multi-drug resistance' do not provide 'pan-drug resistance;' the few that do appear to be associated with poor treatment outcomes.

Cross-resistance between drugs in RCHOP is close to a theoretical minimum

In 1952 Law proposed that if the frequency of resistance by mutation to drug *A* is 10^{-A}, and to drug *B* is 10^{-B}, then only one cell in 10^{A+B} will be simultaneously resistant to both drugs. This assumes that no single mutation confers cross-resistance to both drugs, and therefore represents a theoretical 'best case scenario' with respect to the emergence of multi-drug resistance. We compared our experimentally measured rates of drug resistance to Law's prediction. The frequency of cross-resistance was quantified as a linear combination between the best-case scenario of multiple independent mutations (cross-resistance parameter ξ=0), and a 'worst-case' scenario in which resistance mechanisms overlap to the maximal degree (ξ=1) (68). Several aspects of calculating these frequencies merit discussion. In the mutagenesis and clone tracing experiment, multi-drug resistant clones can arise either by (i) acquisition of a single mutation that confers resistance to more than one drug or (ii) independent acquisition of several mutations each of which confers resistance to a single drug and which in combination confer multi-drug resistance. Only the first case represents true cross-resistance. Thus, the observed frequency

of barcode co-occurrence across multiple drugs represents an upper bound on the actual frequency of single mutations that confer resistance to multiple drugs. Our capacity to experimentally measure cross-resistance was confirmed by performing two independent sets of clone tracing experiments (each in triplicate) for resistance to vincristine (O); although the two experiments involved different drug concentrations and recovery times (to account for variation in these experimental parameters), they demonstrated a high level of cross resistance ($\xi = 0.69$; Supplementary Figure 4). Examining all combinations of 2, 3 or 4 drugs, rates of multi-drug resistance were found to be close to the minimal level of cross-resistance possible (mean $\xi = 0.016$; Figure 7a, b). Thus, the probability that a mutagenized Pfeiffer cell will exhibit resistance to all R-CHOP constituents is not only very low ($<<10^{-6}$) it is near the theoretical minimum given the rate of acquired single drug resistance.

In CRISPR screens, resistance was evaluated by scoring enrichment frequency for the 10 sgRNAs present in the library per gene. This ensures that resistance phenotypes are the result of disruption of the intended gene target and not off-target genes; thus, only true cross-resistance is detected. Law's prediction can still be applied: if resistance to drugs A and B is conferred by a fraction of CRISPR perturbations (at frequencies 10^{-A} and 10^{-B}) then at bare minimum, resistance genes may coincidentally overlap at a frequency of 10^{-A-B}. In CRISPRi and CRISPRa screens, rates of multi-drug resistance deviated somewhat from this assumption, most likely because CRISPR screening yielded genes such as ABC transporters whose physiological function is to protect against multiple xenobiotic stresses. Rates of multi-drug resistance were nonetheless much closer to the best case than worst case scenarios (mean $\xi=0.05$). For example based on the observed rates of single-drug resistance in CRISPRa screens, the theoretical minimum number of 2-drug resistant genes is predicted to be 1 ($\xi = 0$) and the maximum number 132 ($\xi = 1$); the observed average of 18 mutants resistant to a given pair of drugs corresponds to $\xi = 0.13$.

Other applications: hypersensitivity as a guide to vulnerabilities

In addition to providing insight on drug mechanism of action, the identification of genes involved in hypersensitivity has the potential to identify 'collateral sensitivity' interactions, and also druggable vulnerabilities in cancer cells. We analyzed drug hypersensitivity in the same manner as resistance (Methods, Supplementary Figure 7a and 7c). Multiple genes were found to confer hypersensitivity to two different drugs, and three genes conferred hypersensitivity to three drugs; no genes were found that impacted all 4 drugs (Supplementary Figure 7b and 7d). The therapeutic relevance of hypersensitivity data was suggested by one the strongest hits, *LMO2* (LIM domain only 2 gene or T-Cell Translocation Protein 2), whose overexpression by CRISPRa sensitized cells to C and O. High *LMO2* expression is characteristic of the Germinal Center subtype of DLBCL, which responds better to R-CHOP than the low *LMO2* expressing Activated B-Cell subtype (23), and elevated *LMO2* expression is the strongest single gene predictor of overall survival in DLBCL patients treated with CHOP or R-CHOP (69, 70). Our data suggest that the prognostic value of *LMO2* may be mediated in part through its impact on sensitivity to cyclophosphamide and vincristine.

We also investigated the phenomenon of collateral sensitivity, wherein a mutation confers resistance to one drug but heightened sensitivity to another drug. Among 778 CRISPRi or CRISPRa resistance genes, only 13 (1.7%) exhibited hypersensitivity to a different drug. This suggests that collateral sensitivity does not play a major role in R-CHOP therapy: for ~98% of drug resistance mutations, if cells are to be eradicated by R-CHOP it is because they have unchanged sensitivity to at least one other drug. Collateral sensitivity can nonetheless be detected by CRISPRa/i screening and may be relevant to other combination therapies.

To determine if hypersensitivity genes might be addressable therapeutically we asked how many were members of the 'liganded genome' – the subset of proteins known to be bound with high affinity by small molecules (71, 72). We found that 11% of hypersensitivity genes (23 identifiable by CRISPRi

and 49 by CRISPRa) are ligandable. Moreover, 16% of genes whose overexpression confers resistance are liganded, suggesting that molecules targeting resistance mechanisms may be feasible. Study of such compounds and their targets is beyond the scope of the current study but our findings suggest possible avenues to enhance responsiveness to R-CHOP in DLBCL.

DISCUSSION

R-CHOP is an example of a highly successful curative cancer therapy developed over the course of several decades by experimentation in patients. Chemotherapies were combined for the treatment of lymphomas and leukemias based, in part, on theories described by Law and Frei emphasizing suppression of drug resistance as opposed to synergistic pharmacological interaction. In this paper we directly compare pharmacological interaction and suppression of cross-resistance as potential explanations for the superiority of R-CHOP. When tested in three different DLBCL cell lines over a wide range of drug concentrations, no significant synergy was observed among R-CHOP constituents using either Bliss Independence or Loewe Additivity criteria: pairwise drug interactions ranged from additive to antagonistic, and the combined activity of all 5 drugs was close to the expected 'sum of its parts'. The significance of antagonism among R-CHOP components is not clear (and may depend on rates of cell proliferation) but studies of antibiotics have shown that antagonistic drug interactions can be advantageous when the goal is to prevent emergence of drug-resistant mutants (47, 68, 73).

Frequencies and mechanisms of resistance to R-CHOP were investigated using DNA barcoding and CRISPRi/a technology. Large library size (10^6 clones) is a strength of the barcoding approach and it yielded over 10^4 DLBCL mutants resistant (in biological triplicates) to one or more drugs. Barcoding has the drawback that it does not pinpoint genes involved in resistance, and we therefore performed genome-wide CRISPRi/a screens to identify knockout and overexpression phenotypes. For CRISPRi we were able to select for resistance to R, C, H or O in DLBCL cells, but the technical requirements of

CRISPRa limited us to screening for resistance to C, H, and O in chronic myeloid leukemia cells. The results of all three resistance screens were nonetheless clear: among barcoded clones and cells subjected to CRISPRi/a it was possible to isolate progressively fewer clones resistant to one, two, three or four drugs. By barcoding and CRISPRi, no mutants or sgRNAs were found to confer resistance to every drug applied separately. Moreover, the frequencies of multi-drug resistance were close to the theoretical minimum, as defined by the product of empirically determined single-drug resistance frequencies. This was true despite the existence of multi-drug resistance mechanisms, because this study found that most pertain to a subset of drugs, rather than the full combination. In aggregate these data strongly suggest that very low rates of cross-resistance among R-CHOP constituents are key characteristics of the regimen but that synergistic drug interactions are unlikely to play an important role. Our data therefore confirm the hitherto untested theories of Law and Frei (6, 8).

Not all patients with DLBCL are cured by R-CHOP. Some DLBCL cultures are highly resistant to many or all constituent drugs, most likely reflecting variation in drug sensitivity in the human lymphomas from which they were derived. On the basis of the current experiments, it seems unlikely that a DLBCL sensitive to a minority of the drugs in R-CHOP will experience a sufficient depth of killing to eradicate all clones and be cured. Consistent with this idea, our CRISPR screens showed that overexpression of GCLC confers simultaneous resistance to C, H, and O, and high expression of GCLC is significantly associated with poor survival in patients with DLBCL treated by R-CHOP (67). However, multiple R-CHOP resistance and hyper-sensitizing genes are members of the ligandable genome and it may therefore be feasible to develop drugs that increase the fraction of DLBCL patients in whom cures can be achieved.

The current work is performed in cultured cells and it is likely that the components of R-CHOP can interact in different ways in human patients. For example, rituximab is cytotoxic to DLBCL by multiple mechanisms, including signaling-induced cell death, complement-mediated cytotoxicity

(CMC), and antibody dependent cellular cytotoxicity (ADCC) (27). In this study we only score CMC by rituximab since DLBCL cultures displayed little direct induction of apoptosis, and ADCC reconstituted *in vitro* by addition of peripheral blood mononuclear cells elicits insufficient cell death for selection of resistant clones (ie. less than 50% killing at saturating rituximab dose (74, 75)). We cannot exclude the possibility that ADCC interacts synergistically with chemotherapy but note that the immunosuppressive effects of chemotherapy disfavor this hypothesis. With regard to the evolution of drug resistance, Rituximab may behave as though it is several drugs in one if there exist different mechanisms of resistance for killing by CMC, ADCC, and direct cytotoxicity (although CD20 loss constitutes a shared resistance mechanism in all cases) (Figure 7c). This might contribute to the large improvement in DLBCL cure rates that followed addition of Rituximab to CHOP (76). Prednisone, the pro-drug of prednisolone, can induce remissions of DLBCL even as a single agent (30), although such cytotoxicity was not evident in cell cultures. However, the type of pharmacological and cross-resistance studies performed here require molecular manipulations and wide-dose ranges that can only be performed in culture, and evidence that an animal model (or patient) benefits from combination therapy does not discriminate among alternative mechanisms of benefit. As the assessment of synergistic drug interaction is primarily performed in culture, our analysis of R-CHOP remains directly relevant to the pre-clinical development of future drug combinations.

The identification of synergistic drug cocktails is currently perceived as an essential step in development of useful combination therapies (77-79). As discussed above, the dose response of DLBCL to R-CHOP is close to additive, but this is nonetheless a basis for therapeutic superiority over monotherapy from a purely pharmacological perspective. Dose response functions for an *N-plex* combination (*N* between 2 and 5 for parts of R-CHOP) resemble those of an *N*-fold higher dose of monotherapy (Figure 2c); this is dose additivity. In practice, considerations of toxicity prohibit the use of higher dose monotherapy but when the constituents of a combination have qualitatively different

toxicities (as in R-CHOP (80)) additivity allows high-dose conditions to be achieved. The result is greater cell killing at acceptable toxicity.

These results do not mean that drug additivity is a sufficient explanation for cures. A limitation of all tests for pharmacological interaction is they pertain to doses near the IC_{50} value and are therefore relevant to the most drug-susceptible part of a cell population (stronger thresholds may be chosen but viability measurements become noisy below 1%). The primary obstacle to cure in most settings is thought to be acquired drug resistance caused by rare resistance mutations, which can arise even at very high doses. Indeed, early clinical and experimental tests of cancer chemotherapy found that monotherapy did not achieve lasting benefit because it imposed Darwinian selection for drug resistant mutants (81, 82). Following the example set by multi-drug cures for tuberculosis, it was proposed that lasting remission required combined use of chemotherapies each subject to different mechanisms of resistance (see retrospective by (1)). Recent mathematical models of tumor evolution support these ideas, and predict that curing a cancer requires non-cross-resistant drug combinations (83). Unfortunately, systematic analysis of cross-resistance is very difficult using conventional cell culture techniques (7), perhaps explaining why the 'non-overlapping resistance' hypothesis is rarely explored in pre-clinical drug development. With the introduction of clone tracing and genome-wide CRISPR technologies cross-resistance can easily be studied for any new combination therapy active in cultured cells.

If synergistic drug interaction is unnecessary for clinical success, what principles should be used to create new cancer therapies? In the treatment of DLBCL by R-CHOP, the accumulation of log-kills by multiple potent and independently acting drugs exhibiting low levels of cross-resistance appears to be a key principle (Figure 7c). The consequence of high single-agent activity and low cross-resistance is that few clones will resist multiple agents, increasing the likelihood of cure. This idea is consistent with historical reasoning but differs from current approaches that seek to combine drugs with the greatest

synergistic interaction (e.g. (84)). The relevant activity ranges for anti-cancer drugs are difficult to estimate from pre-clinical models because toxicity in the human patient determines tolerable dose and thus, maximum effect. Achieving drug additivity in the context of non-overlapping toxicity as in R-CHOP can be an effective way to achieve levels of cell killing in patients not accessible to monotherapy. The developers of the clone tracing system used here have already suggesting that it be applied to identify combination regimens with non-overlapping resistance (11). The properties of R-CHOP provide strong support for this idea and argue that direct measurement of drug cross-resistance should become as routine in pre-clinical cancer pharmacology as pharmacological interaction. Further use of both methods to study the mechanistic basis of existing curative therapies is also likely to prove informative.

Acknowledgments: We thank F. Stegmeier and C. Bhang for ClonTracer, and A. Letai and A. Eberly Puleo for rituximab. We thank F. Stegmeier, C. Bhang, A. Letai, M. Chung, L. Albacker, L. Maliszewski, M. Cokol, S. Chopra, and K. Subramanian for helpful discussions.

Funding: This work was supported by NHMRC Early Career Fellowship (to A.C.P.), NIH grant P50-GM107618 and U54-CA225088 (to P.K.S.).

Author contributions: Experiments and analysis, A.C.P and C.C.; writing, A.C.P., C.C, and P.K.S.

Competing interests: The authors declare no competing interests.

METHODS

Cell culture and chemotherapies

Diffuse Large B-Cell Lymphoma (DLBCL) cell lines were obtained from the American Type Culture Collection (ATCC) and the Dana Farber Cancer Institute. Identity of Pfeiffer cell line (ATCC® CRL-2632) was validated by Promega GenePrint 10 small tandem repeat (STR) profiling. All DLBCL cell lines were grown in RPMI-1640 with 25 mM HEPES and 2 mM L-alanine-L-glutamine (GlutaMAX) (Gibco 72400), supplemented to 4.5 g/L D-glucose, 10% (v/v) heat inactivated fetal bovine serum (FBS) (Gibco 16140071), and penicillin/streptomycin (P/S) at final concentrations of 100 U/mL and 100 µg/mL, respectively (Corning 30-002-CI). For CRISPRi screens, Pfeiffer cells were grown in RPMI-1640 (Gibco 72400) supplemented with 15% (v/v) FBS and P/S. K562 cells were grown in RPMI-1640 (ATCC 30-2001) with 10 mM HEPES, 4.5 g/L D-glucose, 2 mM L-glutamine, 1 mM sodium pyruvate, and supplemented with 10% (v/v) FBS and P/S. HEK293T cells were grown in Dulbecco's modified Eagle medium (Corning 10-013) with 4.5 g/L D-glucose, 4 mM L-glutamine, 1 mM sodium pyruvate, and supplemented with 10% (v/v) FBS and P/S. All cell lines were grown at 37 °C and 5% CO_2. Cells were tested for mycoplasma contamination using the MycoAlert mycoplasma detection kit (Lonza). When treating with rituximab alone or in combination, media was additionally supplemented with 5% (v/v) pooled complement human serum (HCS) (Innovative Research IPLA-CSER) to enable complement-mediated cytotoxicity. Cells were grown in vented tissue-culture treated polystyrene flasks. Cell density and viability was assessed during culture by a TC20 automated cell counter (Bio-Rad) with trypan blue; all cell densities reported here refer to the count of live cells with diameter between 8 and 24 µm. During culture before drug treatment experiments, DLBCL cells were maintained at the following densities: Pfeiffer between 3×10^5 and 15×10^5 cells/mL; SU-DHL-4 and SU-

DHL-6 between 2×10^5 and 10^6 cells/mL; with centrifugation and transfer to fresh media every 2 to 4 days.

Chemotherapies were obtained as follows: 4-hydroperoxy-cyclophosphamide from Niomech (D-18864), doxorubicin, vincristine, and prednisolone from Selleck (S1208, S1241, and S1737), and rituximab from Dana Farber Cancer Institute. Single-use aliquots of 4-hydroperoxy-cyclophosphamide were prepared in DMSO at -80°C, other chemotherapies were prepared in DMSO and stored at -20°C, and rituximab was prepared at 8 mg/mL in the clinical formulation plus 10% glycerol and stored at 4 °C. DMSO was obtained from Sigma (D2650) and puromycin from Gibco.

Measurement of drug-drug interactions

All drug interaction experiments were conducted in biological duplicates using two independent cultures of the same cell line. After being split from a common ancestor, cultures were propagated in parallel for at least one week before any experiment. Dose responses to single or multiple drugs were measured on DLBCL cells grown in sterile black polystyrene 384-well assay plates. Each well was inoculated with 30 μL of culture at density 10^5 cells/mL, and promptly afterwards concentration gradients of drugs were added to wells by D300 digital dispenser (Hewlett-Packard). All chemotherapies were dispensed as DMSO solutions, while rituximab was prepared at 2.5 mg/mL with 0.05% (v/v) Triton X-100, with a 90 s incubation after pipetting into the print cassette for liquid to be drawn into the print head. At the highest dispensed concentration of rituximab, this conferred a final Triton X-100 concentration of 3 parts-per-million, which we confirmed did not by itself inhibit the growth of DLBCL cells. Wells on plate edges were filled but not used for any measurements. The drug dispensing arrangement of each plate was spatially randomized (and re-organized during data analysis); thereby any spatial bias across a plate becomes random error rather than systematic error across dose responses. Whole control plates of untreated cultures demonstrated no detectable row bias or column bias. Each plate contained >40

untreated wells in randomized locations (not on edges) that served as no-inhibition controls. Assay plates were incubated at 37 °C with 5% CO_2, inside containers humidified by sterile wet gauze. After 72 h, plates were removed from incubation and cooled at room temperature for 30 min, before automated dispensing (BioTek EL406) of 30 µL of CellTiter-Glo (1:1 dilution in phosphate buffered saline (PBS)) into each well. Following a 10 min incubation at room temperature, each well's luminescence was measured in a plate reader (BioTek Synergy H1). At the time of the 384-well plates' initial seeding, 1.5 mL cultures in 6-well plates were prepared from the same cell suspension, with separate cultures including or excluding 5% HCS. At the time of drug addition to plates, one of each such culture was harvested, and cell density was counted (Bio-Rad TC20 using trypan blue), and 72 h later (at the time of CellTiter-Glo addition to 384-well plates) another such untreated 1.5mL culture was harvested and counted. From these density measurements we calculated the number of cell divisions occurring during the time of the assay, which was used during data analysis to determine Growth Rate (GR) metrics (36). Specifically, we used GR = $\log_2$[(relative viability after treatment, according to CellTiter Glo) × (cell number per µL of untreated control culture at t=72 h) / (cell number per µL of untreated control culture at t=0)] / $\log_2$[(cell number per µL of untreated control culture at t=72 h) / (cell number per µL of untreated control culture at t=0)] (Supplementary Figure 1d). By this measure GR=1 indicates full, uninhibited growth, GR=0 indicates complete growth arrest, or that proliferation and death are in balance (final cell count = initial cell count), and GR<0 indicates net cytotoxicity (final cell count < initial cell count); note that we did not impose an asymptotic lower bound of -1 as described by Hafner et al (this would be computed as $2^{GR} - 1$).. HCS slightly speeded the division rate of Pfeiffer in the absence of drugs (17% shorter doubling time), and slightly diminished Pfeiffer sensitivity to 4HC. Pairwise drug interactions (Figure 1) were measured over an 11×11 'checkerboard' of logarithmically-spaced drug concentrations (5 points per order of magnitude), with 5% HCS in media only in interactions with rituximab (for this reason 4HC is less potent in its isobologram with rituximab). The

concentration range for each drug was selected based on preliminary dose-ranging studies so as to span a range from no detectable effect on growth to 98% reduction in cell number relative to untreated control cells, which corresponds to growth arrest plus 90% cell killing. High-order drug interactions, including pairs (Figure 2), were measured over 14-point concentration gradients of one to five drugs, in all cases including 5% HCS so that drug sensitivity and drug-free cell division rate was consistent across conditions that would be compared in analysis. For these high-order interactions, each independent culture (biological replicate) was measured with cultures seeded into duplicate plates (plate-to-plate technical duplicates). Each of these four combinatorially complete drug response sets spanned two 384-well plates, which each contained a full set of single-drug gradients, and thus single-drug responses were in total measured in octuplicate. In the analysis, '100% luminescence' was defined on a per-plate basis by the interquartile mean of at least 50 drug-free wells within that plate (excluding edges). For isobologram analysis (Figure 1), the topology of drug response over the 11×11 checkerboards was smoothed by a nearest-neighbor median filter; this will apply no change to a monotonic response surface, and only smoothes data in cases of locally non-monotonic (that is, jagged) dose response. The absence of this filter changes no conclusions regarding interaction types but yields occasionally jagged isoboles.

Production of ClonTracer lentivirus

ClonTracer library was a gift from Frank Stegmeier (Addgene 67267). Lentiviral particles carrying ClonTracer were produced by calcium phosphate transfection of HEK293T cells (grown in DMEM with 10% fetal bovine serum and 10 mM HEPES) with ClonTracer plasmid (10 μg per 10 cm dish) and lentiviral packaging and VSV-G plasmids psPAX2 and pMD2.G (Cellecta CPCP-K2A; 10 μg of mix per 10 cm dish). Supernatants of transfected HEK293T cells were harvested at 48 h and again at 72 h post-transfection. Supernatants were pooled and clarified by centrifugation (500 ×g, 10 min; keeping

supernatant and discarding pellet). Lentiviral particles were concentrated from supernatant by mixing 3 parts supernatant with 1 part Lenti-X concentrator solution (ClonTech 631231), incubating overnight at 4 °C, centrifuging at 1500 ×g and 4 °C for 45 min, removing supernatant, and resuspending pellet at 1/100 original volume in PBS.

DNA Barcoding of cell lines

10^8 Pfeiffer cells in complete media were treated with 100 μg/mL N-ethyl-N-nitrosourea (ENU) for 4 h; this was previously determined to be the highest dose tolerable by Pfeiffer for this duration without conferring detectable cell death. Cells were washed twice and returned to drug-free media for 72 h to recover. 10^7 of these cells were infected with the ClonTracer lentiviral library by 'spinoculation'. In this protocol, five microcentrifuge tubes were prepared containing 2×10^6 cells in 1 mL complete media, with 8 μg/mL polybrene, and lentivirus at a volume yielding a multiplicity of infection (MOI) of 0.1 (per tube, this was 5 μL of 100× concentrate of lentivirus containing supernatant; see measurement of MOI below). Tubes were incubated for 10 min (37°C, 5% CO_2), and centrifuged at 800 ×g and 37 °C for 60 min. The supernatant was removed, and each cell pellet was resuspended in 4 mL complete media (density 5×10^5 cells/mL) and transferred to one well of a 6-well plate for continued growth (incubation at 37 °C, 5% CO_2). Volume of lentivirus to produce this MOI had been previously determined by test infections of Pfeiffer with different volumes of lentiviral solution, after which the fraction of infected Pfeiffer cells were counted by flow cytometric analysis of the red fluorescent protein encoded by the ClonTracer cassette (BD LSRII, ex:488nm, em:575/26nm), having first gated out dead cells (Violet Viability kit, ThermoFisher L34958, ex:405nm, em:450/50nm) (note, red fluorescence was not readily detectable until 2 days post-infection). From the measured fraction of fluorescent cells, MOI was calculated assuming a Poisson distribution of infection events. Cells were expanded in complete media for 3 days before applying selection for infected cells (which carry a puromycin resistance gene in the

ClonTracer cassette): 3 days in 0.25 μg/mL puromycin, 3 days in 0.5 μg/mL, and 2 days in 1 μg/mL puromycin. At this time flow cytometry could not detect a peak of non-fluorescent cells. Barcoded Pfeiffer cells were grown without puromycin for an additional 4 days before selection experiments in R-CHOP.

Selection for drug resistant clones

From a well-mixed suspension of barcoded Pfeiffer cells, 10^8 cells were harvested and frozen for measurement of pre-treatment DNA barcode frequencies by sequencing. From the same suspension of cells and at the same time, 15 replicate cultures were prepared in 75 cm^2 flasks with 25 mL of complete media containing 5×10^5 cells/mL of barcoded Pfeiffer cells. The total count of 12.5×10^6 cells per flask is calculated to contain 99.999% of the 10^6 unique clones assuming equal initial abundance and random assortment into flasks. Because rituximab displayed an 'inoculum effect' with limited cytotoxicity at high cell density, 3 cultures for rituximab treatment were prepared at lower density and higher volume: 60 mL of barcoded Pfeiffer at 1×10^5 cells/mL in 150 cm^2 flasks, in media supplemented with 5% HCS. The total count of 6×10^6 cells in each rituximab-treated flask is calculated to contain 99.7% of the 10^6 clones. For each drug, and DMSO control, three replicate flasks were treated for 72 h at the following concentrations: 4 μM 4HC; 50 nM doxorubicin; 5.6 nM vincristine; 16 μg/mL rituximab; 0.04% (i.e, 0.0004) (v/v) DMSO (the highest DMSO concentration delivered with any drug). These drug concentrations were chosen on the basis of preliminary dose-finding experiments that identified them to be the highest concentration, in a series of 2-fold concentration steps, from which any surviving cells repopulated the culture within 2 weeks of recovery following the 72 h drug treatment. Following treatment, cultures were washed twice and resuspended in drug-free media. During recovery, culture volumes were adjusted to maintain cell density within the recommended range ($3\text{-}15\times10^5$ cells/mL). No cells were disposed of except from the DMSO control flasks, which suffered no inhibition but were

maintained for a 'recovery' time to match drug-treated flasks. Following recovery to a population size twice the initial inoculum, the recovered cultures were exposed to repeat treatments (each flask treated by the same drug as before), and recovery. Following the second recovery, cultures were centrifuged and cell pellets harvested for barcode sequencing. Prednisolone treatments were designed differently because it was not cytotoxic to cultured Pfeiffer cells (nor any of six other DLBCL cell lines) in concentrations up to 50 μM. Therefore, triplicate Pfeiffer cultures (25 mL in 75 cm^2 flasks) were maintained in 20 μM prednisolone for 20 days, with cell density maintained between 3-15×10^5 cells/mL and with fresh prednisolone administered with media changes every 72 to 96 h (Supplementary Figure 4a). This treatment duration was estimated to produce ≈20-fold enrichment of clones fully resistant to the mild inhibitory effect of prednisolone (≈13 divisions in 20 days ⇒ enrichment from resisting 20% growth inhibition = $(1 / 0.8)^{13}$ = 18-fold).

Barcode amplification and sequencing

To avoid contamination of pre-amplification materials with amplified DNA barcodes (which are approximately a billion-fold more concentrated), all materials, processes and equipment used prior to PCR amplification of ClonTracer barcodes were physically and temporally quarantined from all materials, processes and equipment used following PCR (distant benches and equipment, never both used on the same day). Genomic DNA (gDNA) was extracted from frozen cell pellets with DNeasy Blood and Tissue extraction kits (Qiagen 69504), using the spin-column protocol including RNase A incubation. Four spin columns were used per sample of 10-15×10^6 cells; whereas the pre-treatment sample was a larger population of 3×10^7 cells applied to 8 spin columns. DNA concentration was measured by SYBR green fluorescence with a λ dsDNA calibration curve (readings on BioTek Synergy H1). ClonTracer DNA barcodes consist of a repeating 'Strong (G or C) - Weak (A or T)' pattern with no detectable PCR amplification bias so that barcode counts measured by deep sequencing are proportional

to clone abundance (11). Barcodes were amplified from 20 μg of gDNA per sample, representing 3 million diploid genomes as template, with Q5 polymerase (New England Biolabs M0492). This was accomplished with parallel 50 μL reactions with 2 μg of template each. The pre-treatment sample was amplified from 20μg of DNA, representing 6 million genomes. Primer sequences were as described previously (see Supplementary Table 2 of Bhang*, et al.* (11)). Reaction success and yield was verified by agarose gel electrophoresis. PCR products of all treatment conditions were pooled and size selected (133 bp) by excision from an agarose gel (using SYBR-safe stain and blue LED illumination) with purification by QIAquick Gel Extraction Kit (Qiagen 28704). PCR product from pre-treatment cell sample was processed separately rather than pooled with others. PCR products were sequenced on Illumina HiSeq 2500 in high-output single read mode, with custom read (CCGAGATACTGACTGCAGTCTGAGTCTGACAG) and index (AGCAGAGCTACGCACTCTATGCTAG) primers. A 30% PhiX spike-in provided necessary sequence diversity. FASTQ files were analyzed by the clonTracer_analyze v1.0 script which is available with the ClonTracer system (see www.addgene.org, cat. #67267). This script conducts the Barcode-composition analysis described by Bhang*, et al.* (11), which identifies high-quality reads that conform to the expected barcode pattern (30nt of alternating weak (A/T) then strong (G/C)), and merges barcode sets that contain one high abundance barcode and sequence-adjacent barcodes (hamming distance 1 or 2) at much lower abundance indicating that they are sequencing errors of the high-abundance barcode. For each drug treated sample, 6-8×10^6 barcode reads were obtained, and from the pre-treatment sample 1.6×10^8 barcode reads were obtained; the latter being sequenced at greater depth.

Analysis of barcode enrichment

Barcode counts in the pre-treatment sample were assigned a lower bound of the 5% quantile of counts in this sample (34 counts); this prevents barcodes that were rare or undetected in the pre-treatment sample

from scoring as highly enriched in a drug treatment while having, for example, only 2 reads. Absolute barcode counts in pre- and post-treatment samples were then converted to the fraction of all counts for that sample. Each barcode's enrichment in a given drug treatment was calculated as post-treatment frequency divided by pre-treatment frequency. The biological triplicates of each treatment were merged to a single score by calculating the geometric mean enrichment. Each repeat was assigned a minimum enrichment of 1 when calculating geometric mean, to prevent severely penalizing barcodes that were not detected in one of three repeats; this is motivated by the statistical possibility that a barcode may be absent from any one flask's inoculum. A small fraction of barcodes exhibited geometric mean enrichment >1 in DMSO-treated cultures (1% of barcodes were enriched ≥ 10-fold), and therefore to normalize for these differences in fitness that are unrelated to drug sensitivity, we divided each barcode's enrichment scores in drug treatments by its enrichment in DMSO only when DMSO-enrichment was greater than 1 (enrichment scores in a drug treatment were not increased by having DMSO enrichment score less than 1).

Lentivirus production for CRISPR reagents

HEK293T cells were transfected with the lentiviral plasmid of interest (as mentioned in relevant sections below), psPAX2 (Addgene #12260) and pCMV-VSV-G (Addgene #8454) in a 2:2:1 molar ratio using lipofectamine 3000 (Invitrogen) according to the manufacturer's instructions. The growth medium was replaced 6 h post-transfection and was then harvested at 28 h and 52 h post-transfection. The two harvested growth medium fractions were pooled, centrifuged at 1000 ×g for 10 min, and filtered through a 0.45 μm low-protein binding membrane. Lentivirus containing supernatants were stored at -80 °C. If needed, lentivirus titers were increased by adding ViralBoost reagent (Alstem) to the cell culture medium and lentivirus supernatants were concentrated using a lentivirus precipitation solution (Alstem).

Generation of Cas9-expressing cell lines

To generate the Pfeiffer cell line stably expressing dCas9-KRAB (Pfeiffer CRISPRi), Pfeiffer cells (ATCC CRL-2632) were transduced with lentiviral particles produced using vector pMH0001 (Addgene #85969; expresses dCas9-BFP-KRAB from a spleen focus forming virus (SFFV) promoter with an upstream ubiquitous chromatin opening element) in the presence of 8 µg/mL polybrene. A pure polyclonal population of dCas9-KRAB expressing cells was generated by 3 rounds of fluorescence activated cell sorting (FACS) gated on the top half of BFP positive cells (BD FACS Aria II).

To generate the K562 cell line stably co-expressing dCas9 fused to the SunTag, and a SunTag-binding antibody fused to the VP64 transcriptional activator (K562 CRISPRa), K562 cells (ATCC CCL-243) were first transduced with lentiviral particles produced using vector pHRdSV40-dCas9-10xGCN4_v4-P2A-BFP (Addgene #60903; expresses dCas9 tagged with 10 copies of the GCN4 peptide v4 and BFP) in the presence of 8 µg/mL polybrene. After selection of BFP positive cells using one round of FACS (BD FACS Aria II), cells were transduced with lentiviral particles produced using vector pHRdSV40-scFv-GCN4-sfGFP-VP64-GB1-NLS (Addgene #60904; expresses a single chain variable fragment (scFv) that binds to the GCN4 peptide from the SunTag system, in fusion with a green fluorescent protein (GFP) and VP64) in the presence of 8 µg/mL polybrene. Single cells with high GFP levels (top 25% of GFP positive cells) and high BFP levels (top 50% of BFP positive cells) were isolated by FACS and grown in single wells of a 96-well plate. Monoclonal cell lines were expanded and tested for their ability to increase the expression of target control genes (explained below). A single clone exhibiting robust growth and robust overexpression of target genes was selected as cell line K562 CRISPRa.

Evaluation of CRISPRi/a cell lines using sgRNAs targeting individual genes

Pairs of complementary synthetic oligonucleotides (Integrated DNA Technologies) forming sgRNA protospacers flanked by BstXI and BlpI restriction sites were annealed and ligated into BstXI/BlpI double digested plasmid pU6-sgRNA EF1Alpha-puro-T2A-BFP (Addgene #60955). Protospacer

sequences used to target individual genes and synthetic oligonucleotides are listed in Table S1. The sequence of all sgRNA expression vectors was confirmed by Sanger sequencing and lentiviral particles were produced using these vectors as described above (see "lentivirus production"). Pfeiffer CRISPRi and K562 CRISPRa cells were infected with individual sgRNA expression vectors by addition of lentivirus supernatant to the culture medium in the presence of 8 µg/mL polybrene. Transduced cells were selected using puromycin (0.8 µg/mL for Pfeiffer and 2 µg/mL for K562) starting 48 h post-transduction and over the course of 7 days with daily addition of the antibiotic. After 24 h growth in puromycin-free medium, 1×10^5 cells were harvested and total RNA was extracted using the RNeasy Plus Mini kit (Qiagen). cDNA was synthesized from 0.1 µg total RNA using Superscript IV reverse transcriptase (Invitrogen) and oligo$(dT)_{20}$ primers (Invitrogen), following the manufacturer's instructions. Reactions were diluted 4-fold with H_2O and qPCR was performed in 10 µL reaction volume in 96-well plates using PowerUp SYBR Green PCR Master mix (ThermoFisher Scientific), 2 µL diluted cDNA preparation, and 0.4 µM of primers. All qPCR primers are listed in Table S1. To calculate changes in expression level of target genes, all gene specific Ct values were first normalized to the Ct value of a reference gene (GAPDH) to find a ΔCt value. Log_2 fold changes in expression were then determined by the difference between the ΔCt value of targeting sgRNAs and that of a non-targeting negative control sgRNA (ΔΔCt).

CRISPRi/a screens

Genome-wide libraries of sgRNAs from Addgene (hCRISPRi_v2: #83969 and #83970; hCRISPRa_v2: #83978 and #83979; a gift from Jonathan Weissman (53)) were amplified in MegaX DH10B T1R cells (Invitrogen). These two libraries are provided as two sub-libraries each containing about 100,000 individual plasmids (5 sgRNAs per gene). Sub-libraries (100 ng) were electroporated into MegaX DH10B T1R cells according to the manufacturer's instructions and the resulting transformed cells were

plated on 10× 150 mm LB/Ampicillin (100 μg/mL) Petri dishes. After 17 h at 30 °C, cells were scraped off the plates, washed with LB, and plasmid DNA was prepared from the cell pellet using the Plasmid Plus Maxi kit (Qiagen). Coverage for each sub-library was determined by serial dilution and colony counting, and was at least 5,000× for each sub-library. Lentiviral supernatant was prepared using an equimolar ratio of each sub-library plasmid for both the hCRISPRi_v2 and the hCRISPRa_v2 sgRNA libraries as described above ("lentivirus production") and was stored at -80 °C. The multiplicity of infection (MOI) of both preparations was determined by titration onto the target cell line and quantification of the percentage of BFP positive cells 2-3 days post-transduction by flow cytometry (BD Biosciences LSR II).

For CRISPRi screens, Pfeiffer CRISPRi cells (2.5×10^8) were transduced with the hCRISPRi_v2 library lentivirus at an MOI of 0.4 in 250 mL culture medium + 8 μg/mL polybrene in 3× 225 cm^2 cell culture flasks (Costar). 24 h post-transduction, cells were harvested and resuspended in 400 mL fresh medium in 4× 225 cm^2 cell culture flasks. Starting 48h post-transduction, the culture medium was exchanged daily and cells were maintained at 0.8×10^6/mL in puromycin (0.8 μg/mL) in 400-500 mL. After 5 days in puromycin, the proportion of BFP positive cells determined by flow cytometry increased from 37% to 90% of the fraction of viable cells. After recovery for 1 day in puromycin-free medium, the library cells were ready for initiation of parallel drug selections. First, a T0 sample of 6×10^7 cells was harvested and stored at -80 °C. Each screen was initiated using 6×10^7 cells at 0.4×10^6/mL in 2× 225 cm^2 cell culture flasks. Vincristine (O), 4-hydroperoxy-cyclophosphamide (C), and Doxorubicin (H) were added from 500× stocks in DMSO. A DMSO-only screen was used as an untreated control screen. Rituximab (R) was added from a 2 mg/mL stock in PBS and 5% (v/v) HCS was added to the growth medium. A screen with matching treatment of 5% (v/v) HCS was used as an untreated control screen for rituximab. For the duration of the screen, cells were maintained in 2× 225 cm^2 cell culture flasks at a minimum concentration of 0.4×10^6/mL in 150 mL (minimum coverage of 300 cells per sgRNA) by exchanging the

medium to fresh medium every 2 days. For drug treatment, cells were treated with pulses of drug for 3 days followed by exchange of the growth medium. O (5.0 nM final concentration) was added on day 0, day 7 and day 11; C (3.3 μM) was added on day 0 and day 3; H (27 nM) was added on day 0 and day 7; R (4 μg/mL and 5% HCS) was added on day 0, day 5 and day 10. During the course of the screen, cell count and viability were measured using a TC20 automated cell counter (Bio-Rad) using trypan blue. The vincristine CRISPRi screen underwent 7.60 fewer population doublings than the DMSO control screen; the 4-hydroperoxy-cyclophosphamide screen underwent 9.34 fewer doublings; and the doxorubicin screen underwent 7.41 fewer doublings. The rituximab CRISPRi screen underwent 7.53 fewer population doublings than the 5% HCS control screen. At day 14, 8×10^7 cells were harvested from each screen by centrifugation, washed twice with PBS and gDNA was extracted using the QIAamp DNA Blood Maxi Kit (Qiagen) according to the manufacturer's instruction, except that the elution was performed using 10 mM Tris·HCl pH 8.5. Typical yields from 8×10^7 cells ranged from 500-650 μg gDNA.

For CRISPRa screens, K562 CRISPRa cells (3×10^8) were transduced with the hCRISPRa_v2 library lentivirus at an MOI of 0.25 in 300 mL culture medium + 8 μg/mL polybrene in 3× 225 cm^2 cell culture flasks (Costar). 24 h post-transduction, cells were harvested and resuspended in 450 mL fresh medium in 4× 225 cm^2 cell culture flasks. Starting 48h post-transduction, the culture medium was exchanged daily and cells were maintained at 0.8×10^6/mL in puromycin (1.5-1.75 μg/mL) in 400-500 mL. After 5 days in puromycin, the proportion of BFP positive cells determined by flow cytometry increased from 26% to 96% of the fraction of viable cells. After recovery for 1 day in puromycin-free medium, the library cells were ready for initiation of parallel drug selections. First, a T0 sample of 8×10^7 cells was harvested and stored at -80 °C. Each screen was initiated using 6×10^7 cells at 0.4×10^6/mL in 2× 225 cm^2 cell culture flasks. Vincristine (O), 4-hydroperoxy-cyclophosphamide (C), and Doxorubicin (H) were added from 500× stocks in DMSO. A DMSO-only screen was used as an untreated control screen. For

the duration of the screen, cells were maintained in 2× 225 cm^2 cell culture flasks at a minimum concentration of 0.4×10^6/mL in 150 mL (minimum coverage of 300 cells per sgRNA) by exchanging the medium to fresh medium every 2 days. For drug treatment, cells were treated with pulses of drug for 3 days followed by exchange of the growth medium. O (35.0 nM final concentration) was added on day 0 and day 8; C (7.5 μM) was added on day 0 and day 8; H (27 nM) was added on day 0 and day 8. During the course of the screen, cell count and viability were measured using a TC20 automated cell counter using trypan blue. The vincristine CRISPRa screen underwent 8.80 fewer population doublings than the DMSO control screen; the 4-hydroperoxy-cyclophosphamide screen underwent 10.52 fewer doublings; and the doxorubicin screen underwent 9.87 fewer doublings. At day 15, 8×10^7 cells were harvested from each screen by centrifugation, washed twice with PBS and gDNA was extracted using the QIAamp DNA Blood Maxi Kit according to the manufacturer's instruction, except that the elution was performed using 10 mM Tris·HCl pH 8.5. Typical yields from 8×10^7 cells ranged from 500-680 μg gDNA.

sgRNA barcode sequences were amplified by PCR using the extracted gDNA from either CRISPRi or CRISPRa screens as template and Phusion (NEB M0530) as polymerase. An equimolar mix of primers with stagger regions of different length (CC_LSP_025 to CC_LSP_032) was used as forward primer (to maintain sequence diversity in the common linker region for high-throughput sequencing purposes) and barcoded index primers (CC_LSP_033 to CC_LSP_040) were used as reverse primers. Reactions were composed of 1× HF buffer, 0.2 mM dNTPs, 0.4 μM forward primer mix, 0.4 μM indexed reverse primer, 0.5 μL Phusion, 1.5 mM $MgCl_2$, and 5 μg gDNA in a volume of 50 μL. After initial melting at 98 °C for 30 s, the reactions were subjected to 24 cycles of heating at 98 °C for 30 s, annealing at 62 °C for 30 s and extension at 72 °C for 30 s, and were followed by a final extension step at 72 °C for 5 min. After verification of the PCR reaction success by agarose gel electrophoresis using SYBR safe stain (Thermo Fisher Scientific) on a single 50 μL reaction, 50% of the extracted gDNA for each screen (gDNA from 4×10^7 cells, corresponding to a coverage of 200×) was used as template in PCR reactions

(typically 50-70 reactions per screen). After pooling all reactions from each single screen, the amplified sgRNA barcode PCR product (~240-250 bp) was purified by agarose gel electrophoresis using the QIAquick gel extraction kit (Qiagen). The concentration of individual libraries was quantified by fluorescence using the Qubit dsDNA high sensitivity assay kit (Thermo Fisher Scientific). Individual indexed libraries were mixed in equimolar ratio and were further purified using a QIAquick PCR purification kit (Qiagen). After determining accurate concentrations by quantitative PCR using the NEBnext library quant kit for Illumina (NEB), pooled libraries were sequenced on an Illumina HiSeq 2500 platform using a 50 bp single read on a high output standard v4 flow cell with a 15-20% PhiX spike-in. A total of 51-72 million reads were obtained for each indexed screen (minimum coverage of 250×).

The fastq sequencing files were analyzed using a Python-based ScreenProcessing pipeline previously reported by Horlbeck et al. (https://github.com/mhorlbeck/ScreenProcessing; (53)) with the following modification introduced due to the use of a mix of forward primers with a staggered region of different length. All reads were first processed using Cutadapt (85) to remove the linker sequence in front of the sgRNA barcode in each read (CTTGGAGAACCACCTTGTTG). To count the abundance of each sgRNA barcode in every sample, trimmed sequences were aligned to the library of protospacers present in the hCRISPRi_v2 or hCRISPRa_v2. Typically, 83-87% of the number of raw reads were aligned to the library of protospacers. The count files were next used to generate negative control genes, and calculate enrichment phenotypes and Mann-Whitney p-values as previously described (14, 53). To estimate technical noise in the screen, simulated negative control genes (the same number as that of real genes) were generated by randomly grouping 10 sgRNAs from the pool of ~4000 non-targeting control sgRNAs present in the libraries. The phenotypic effect of each sgRNA was quantified by the rho phenotype metric (54) which calculates the log2 fold change in abundance of an sgRNA between the treated and vehicle control samples, subtracting the equivalent median value for all 4000 non-targeting

sgRNAs, and dividing by the number of population doubling differences between the treated and vehicle control populations. Similarly, untreated growth phenotypes ('gamma' phenotypes) can be calculated by a comparison of vehicle control and T0 samples; and 'tau' phenotypes can be calculated by a comparison of treated and T0 samples (14, 54). For each gene (and simulated control gene), which is targeted by 10 sgRNAs, two metrics were calculated: (i) the mean of the strongest 5 rho phenotypes by absolute value, and (ii) the p-value of all 10 rho phenotypes compared to the 4000 non-targeting control sgRNAs (Mann-Whitney test). For genes with multiple independent transcription start sites (TSSs) targeted by the sgRNA libraries, the two metrics were calculated independently for each TSS and the TSS with the lowest Mann-Whitney p-value was chosen for further analysis. sgRNAs were required to have a minimum of 25 counts in at least one of the two conditions tested to be included in the analysis. To deal with the noise associated with potential low count numbers, a pseudocount of 10 was added to all counts. Genes that had less than 8 sgRNA rho phenotypes were not included for further analysis. Read counts and phenotype scores for individual sgRNAs are available in the Supporting Information. Gene-level phenotype scores and p-values are available in the Supporting Information.

CRISPRi cyclophosphamide hypersensitivity screen

The additional CRISPRi cyclophosphamide screen (Supplementary Figure 5b) for identification of hypersensitive hits was performed and analyzed as described above with the following key modifications. Pfeiffer CRISPRi cells (2×10^8) were transduced with the top 5 half library of hCRISPRi_v2 (Addgene #83969, ie 5 sgRNAs per gene) at an MOI of 0.3 in 200 mL culture medium + 8 µg/mL polybrene in 2× 225 cm^2 cell culture flasks. 24 h post-transduction, cells were harvested and resuspended in 300 mL fresh medium in 3× 225 cm^2 cell culture flasks. Starting 48h post-transduction, the culture medium was exchanged daily and cells were maintained at 0.8×10^6/mL in puromycin (0.6 µg/mL) in 300-400 mL. After 3 days in puromycin, cells were recovered for 1 day in puromycin-free

medium. A T0 sample of 5×10^7 cells was harvested and stored at -80 °C. The CRISPRi screen was initiated using 2.5×10^7 cells at 0.4×10^6/mL in 1× 225 cm^2 cell culture flask. For the duration of the screen, cells were maintained in 1× 225 cm^2 cell culture flask at a minimum concentration of 0.4×10^6/mL in 62.5 mL (minimum coverage of 250 cells per sgRNA) by exchanging the medium to fresh medium every 2 days. 4-hydroperoxy-cyclophosphamide (2.5 μM final concentration) was added on day 0 and day 8. The cyclophosphamide CRISPRi screen underwent 4.38 fewer population doublings than the DMSO control screen. At day 15, gDNA was extracted from 5×10^7 cells from each screen and half of that was used as template in PCR reactions (coverage of 250×). A total of 31-34 million reads were obtained for each indexed screen and 81-82% of those reads were aligned to the reference library of protospacers. Negative control genes were generated by randomly grouping 5 sgRNAs from the pool of ~2000 non-targeting control sgRNAs present in the half-library. For each gene (and simulated control gene), which is targeted by 5 sgRNAs, two metrics were calculated: (i) the mean of the strongest 3 rho phenotypes by absolute value, and (ii) the p-value of all 5 rho phenotypes compared to the 2000 non-targeting control sgRNAs (Mann-Whitney test). Low count numbers were dealt with by adding a pseudocount of 1 to all zero counts. Gene ontology analysis was performed on the full output list of genes ranked by hypersensitivity score using GOrilla (86). The reported p-value is the enrichment p-value computed according to the GOrilla algorithm. The 'FDR q-value' represents the correction of the p-value for multiple testing hypothesis.

Cross-resistance analysis of CRISPR screens

For each gene, a single aggregate resistance score was calculated by multiplying the two metrics determined in the screen processing pipeline (resistance score = $-\log_{10}$(Mann-Whitney p-value)×mean of the strongest 5 rho phenotypes). Genes required 8 or more observed sgRNA rho phenotype scores in a specific screen for inclusion in the analysis. In order to account more accurately for the technical noise

in the screen, 10 random sets of simulated control genes were generated. A resistance score was then calculated for each simulated control gene in all 10 sets for all the drugs tested (4 for CRISPRi and 3 for CRISPRa). Genes that have a resistance score above a specific cutoff in at least 2 conditions tested are defined as 'cross-resistant'. The cutoff for cross-resistance analysis was determined by systematically quantifying the number of simulated control genes that would score as cross-resistant over the full range of resistance score cutoffs (in 0.01 increments). We selected a cutoff that scored on average over the 10 sets of control genes a single (or less than one) double resistant negative control simulated gene over all possible two drug combinations. Cross-hypersensitivity analyses were performed in an analogous way (the hypersensitivity score was calculated in the same way as the resistance score).

Figure 1.

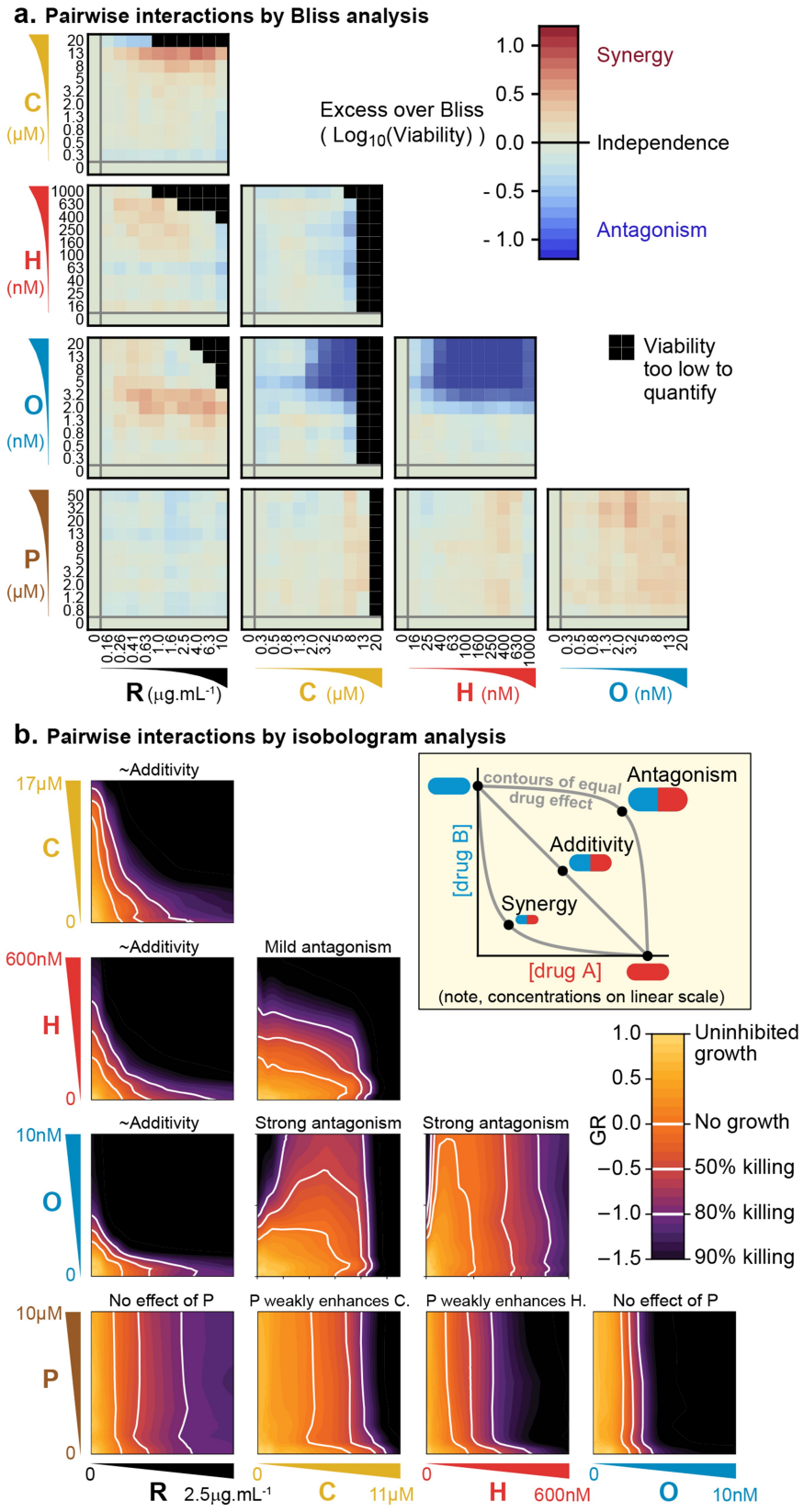

Figure 1. Pairs of drugs in R-CHOP exhibit little synergy, but some strong antagonism, in a Diffuse Large B-Cell Lymphoma cell line. a. DLBCL cells (Pfeiffer) grown in microtiter plates were treated with drug combinations for 72 hours followed by a luminescence-based assay for cell viability. 'Excess over Bliss' measures the observed deviation from Bliss Independence model. **b**. Isobologram analysis of the same drug interaction experiments. For this analysis, luminescence relative to untreated control cells was converted to into a GR metric (36) to distinguish cytostatic from net cytotoxic effects (Supplementary Figure 1d). White contours highlight thresholds equivalent to complete growth inhibition (GR = 0), and complete growth inhibition plus 50% or 80% cell killing (GR<0). Inset: principles of isobologram analysis; isoboles are contours of equal drug effect, which are straight lines in the case of 'additivity'.

Figure 2.

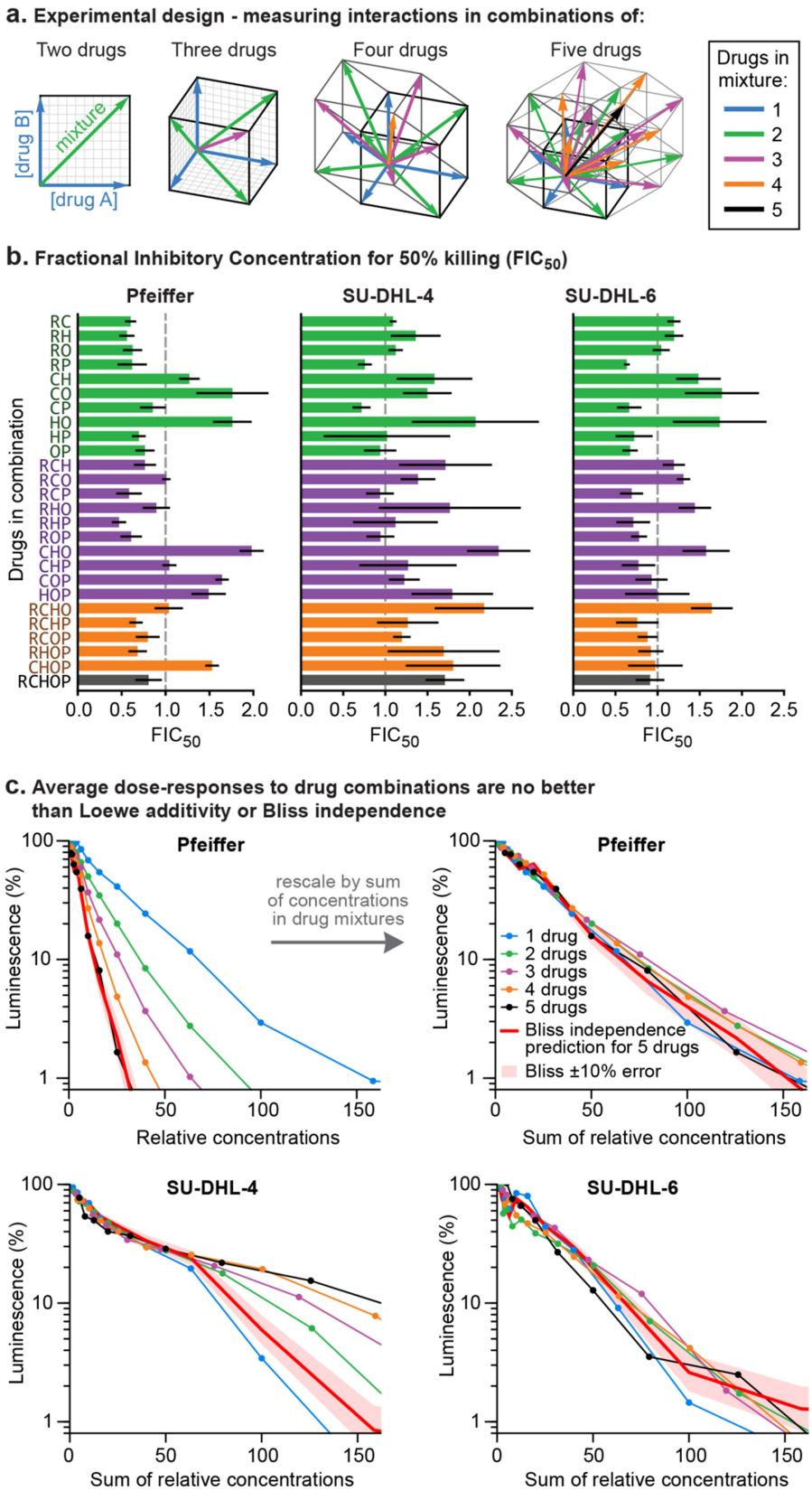

Figure 2. Higher order drug combinations do not exhibit synergistic cell killing. a. Experimental design for measurement of high-order drug interactions. Two or more drugs were mixed in equipotent ratios such that they similarly contributed to cytotoxicity as the dose of the mixture was increased. Dose gradients of drug mixtures span diagonal lines in multi-drug concentration space. **b**. Synergy or antagonism of multidrug combinations was quantified by Fractional Inhibitory Concentrations (FIC, also called Combination Index) at the 50% killing threshold (Supplementary Figure 1d). Given a mixture of drugs at a dose that causes 50% killing, FIC is the sum of each drug's concentration in that mix as a fraction of the single-agent doses producing the same effect: $\mathrm{FIC}_{50} = \sum \frac{\mathrm{IC50}_{\text{drug in combination}}}{\mathrm{IC50}_{\text{drug alone}}}$. FIC=1 indicates Loewe additivity. Error bars are 95% confidence intervals (n = 4 per point along dose response). **c**. Average dose response functions to single drugs or mixtures of different numbers of drugs (i.e, average of single-drug responses; average of drug pair responses, etc). Red line: the expected response to R-CHOP drugs according to the Bliss Independence model; pale red area: ±10% error in number of log-kills around the Bliss Independence model. Top left: Horizontal axis shows the amount of each drug present in a mixture, for example, the combination of 40 units each of drug A and drug B appears at *x*-coordinate 40 (units are scaled to align single-agent activity; Supplementary Figure 2a). Top right, bottom left, bottom right: Horizontal axis is the sum of drug concentrations, for example, the combination of 40 units each of drug A and drug B is plotted at *x*-coordinate 80 (40+40). Alignment of dose response functions indicates that combinations of *N*-many drugs act as an *N*-fold greater dose of monotherapy, which complies with the Loewe Additivity model.

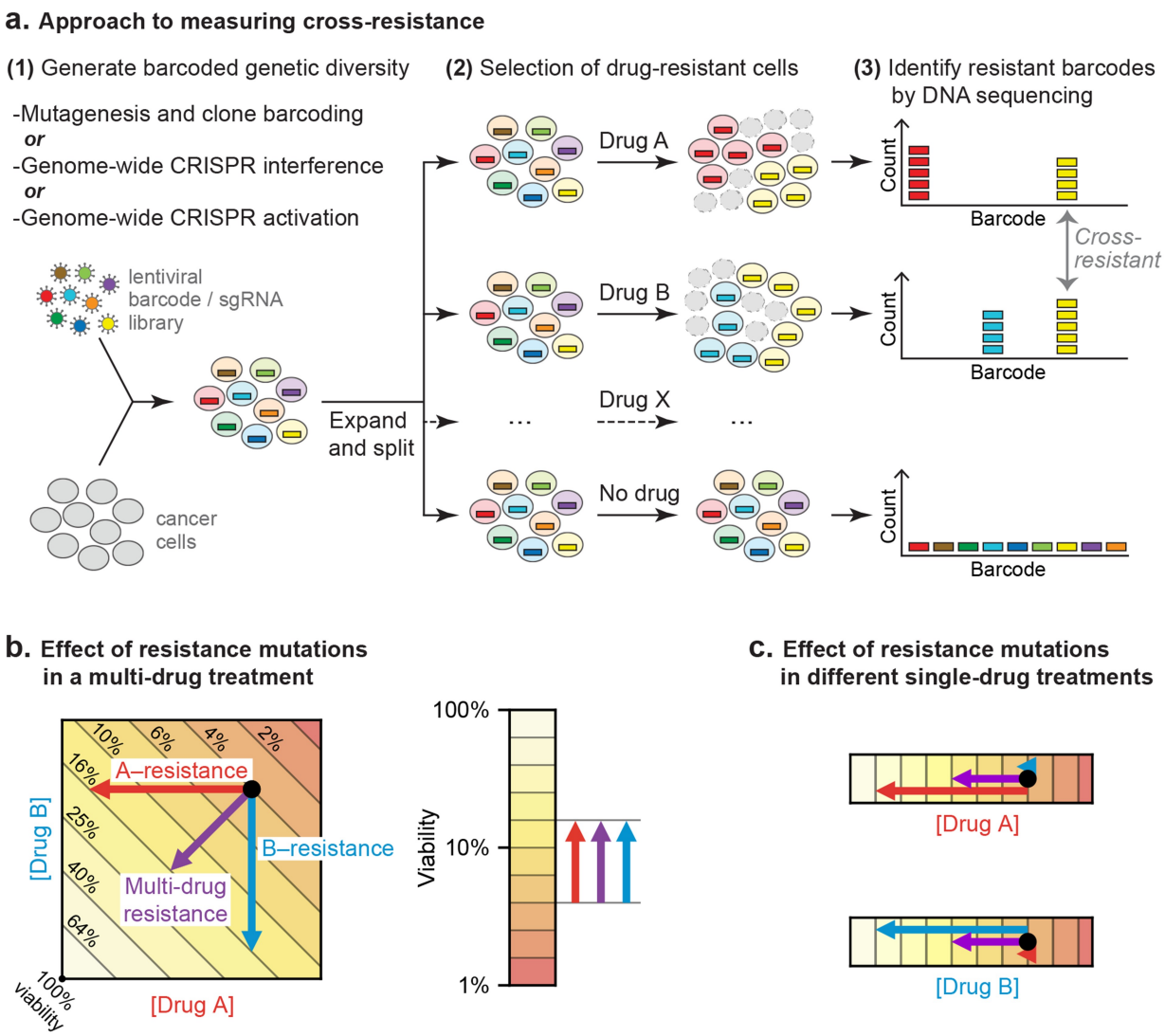

Figure 3. Strategy for measuring cross-resistance between drugs. a. Cells were mutagenized and barcoded using one of three approaches: (i) random mutagenesis and clone tracing, (ii) gene knockdown via CRISPR interference (CRISPRi), or (iii) gene overexpression via CRISPR activation (CRISPRa). Large pools of cells (1 million clones for random mutagenesis; genome-wide perturbation for CRISPRi/a) were expanded and split into replicate cultures, which were then treated with single drugs. The abundance of specific DNA barcodes or sgRNAs in each culture was measured before and after drug exposure by next-generation DNA sequencing. The resistance of cells to drug treatment was scored

based on the degree of barcode enrichment, and cross-resistance was determined by significant enrichment in two or more drug treatments. **b**. Illustration of the need to select for resistance mutations using single drugs rather than cocktails. Arrows: because drug resistance is functionally analogous to lowering the drug concentration, resistance mutations move cells to different coordinates in drug concentration space. Cross-resistance (purple arrow) can have same effect on survival as more penetrant single-drug resistance (red, blue arrows). **c**. By selecting resistance mutations in single drugs, cross-resistance, and the magnitude of the effect on each drug, is clear.

Figure 4.

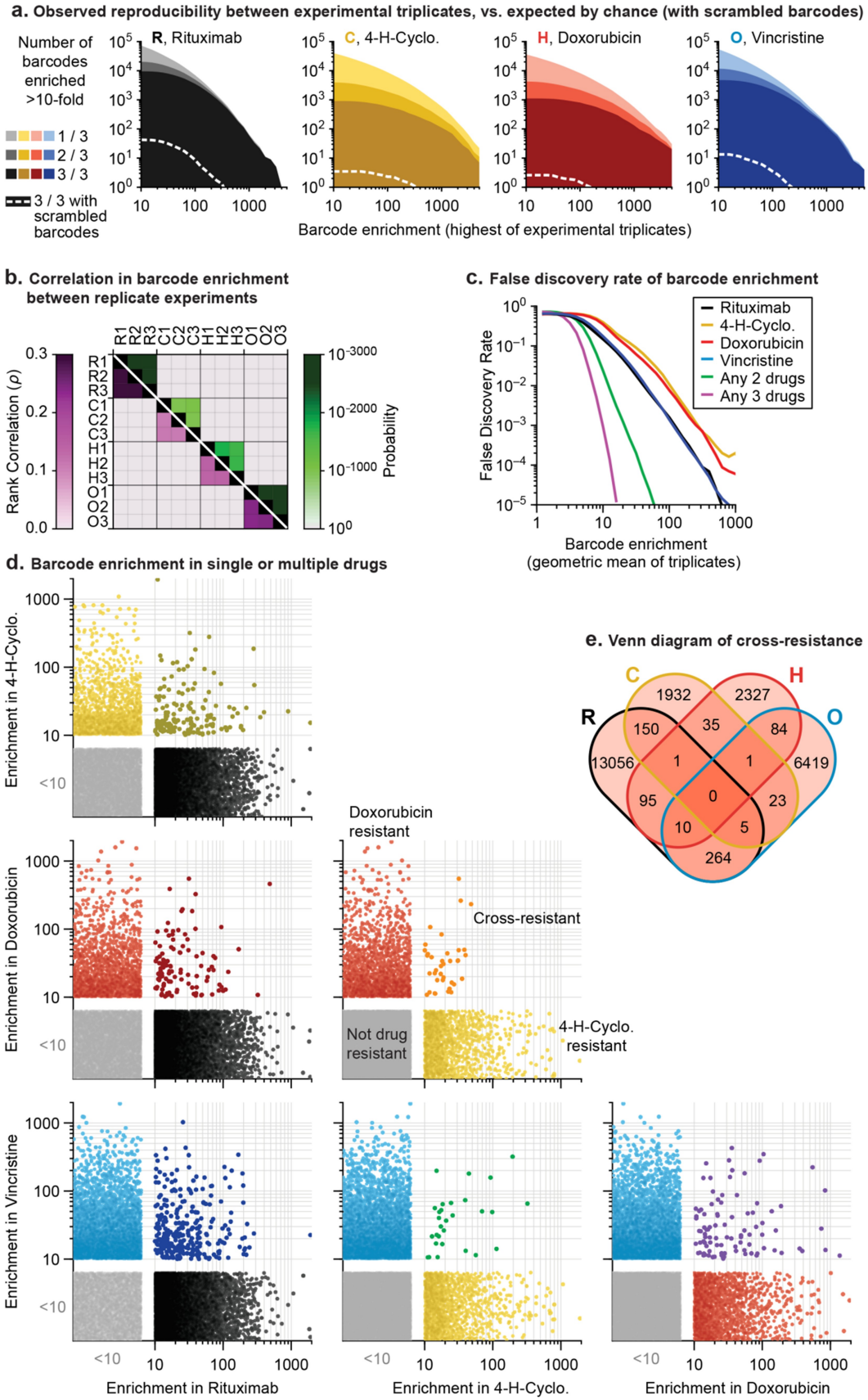

Figure 4. In mutagenized clones single-drug resistance is common but multi-drug resistance rare.

a. Reproducibility of DNA barcode enrichment among drug treatments in triplicate. The enrichment for each barcode in a cell culture exposed to a single drug is its post-treatment read frequency divided by pre-treatment read frequency. Horizontal axis is the highest value for each barcode's enrichment scores in any triplicate. Vertical axis is the number of barcodes for which 1, 2, or 3 triplicates had enrichment ≥ 10. Dashed white line: error model indicating repeated enrichment expected by random chance; see Methods for details. **b**. Matrix of Spearman rank correlation in enrichment scores between drug treatments (ρ in pink scale; one-sided P-value in green scale). **c**. False discovery rate of barcode enrichment, per magnitude of enrichment (geometric mean of triplicates), was computed by comparing observed barcode enrichment to the error model of scrambled barcodes (10^{10} triplicates simulated by scrambling actual data). At geometric mean enrichment = 10, false discovery rate for 2-drug and 3-drug resistance is 2.5% and 0.1%, respectively. **d.** Scatterplots of barcode enrichment scores (geometric mean of biological triplicates for each drug) for each pair of two drugs in RCHO. Each dot represents a single barcode. Enrichment scores below 10 are deemed not significant, and are displayed with scatter in the '<10' region of each axis. **e**. Venn diagram of the number of barcodes exhibiting resistance (geometric mean enrichment ≥ 10) to single or multiple drugs.

Figure 5.

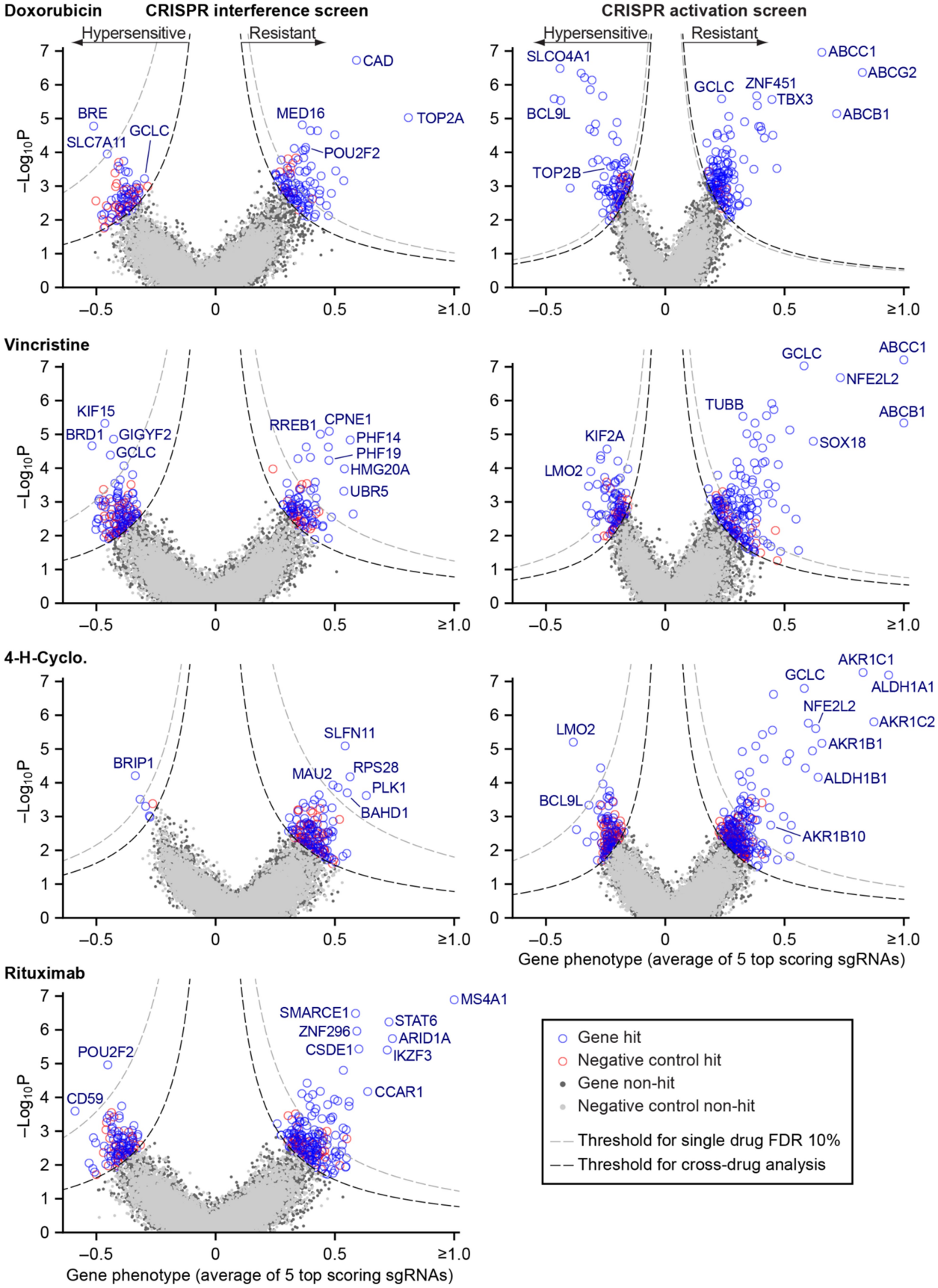

Figure 5. Identification of mechanisms of single drug resistance by genome-wide CRISPRi and CRISPRa screens. Volcano plots of gene phenotype and *p*-value for CRISPRi (left) and CRISPRa (right) screens of single cytotoxic drugs in the R-CHOP regimen. Phenotype of 1 indicates complete drug resistance, 0 indicates parental sensitivity, <0 indicates heightened drug sensitivity. The coordinate of each gene was determined by the average phenotype of the 5 most active sgRNAs targeting that gene (of the 10 per gene) and $-\log_{10}$ of the *p*-value (Mann-Whitney test of phenotypes for all sgRNAs targeting that gene compared to 4000 non-targeting control sgRNAs). Negative control genes were generated by randomly grouping sets of non-targeting controls analyzing as for true genes. Gray dashed line: threshold for 10% false discovery rate (FDR) for single-drug resistance, or hypersensitivity, calculated by comparison to 10 sets of ≈19,000 negative control genes. Black dashed line: threshold for cross-resistance analysis was set at a level that yielded less than one double-resistant negative control gene out of all possible drug pairs (equal to multi-drug resistance FDR 4% for CRISPRi and 2% for CRISPRa). Labeled genes are a non-exhaustive selection of top scoring hits.

Figure 6.

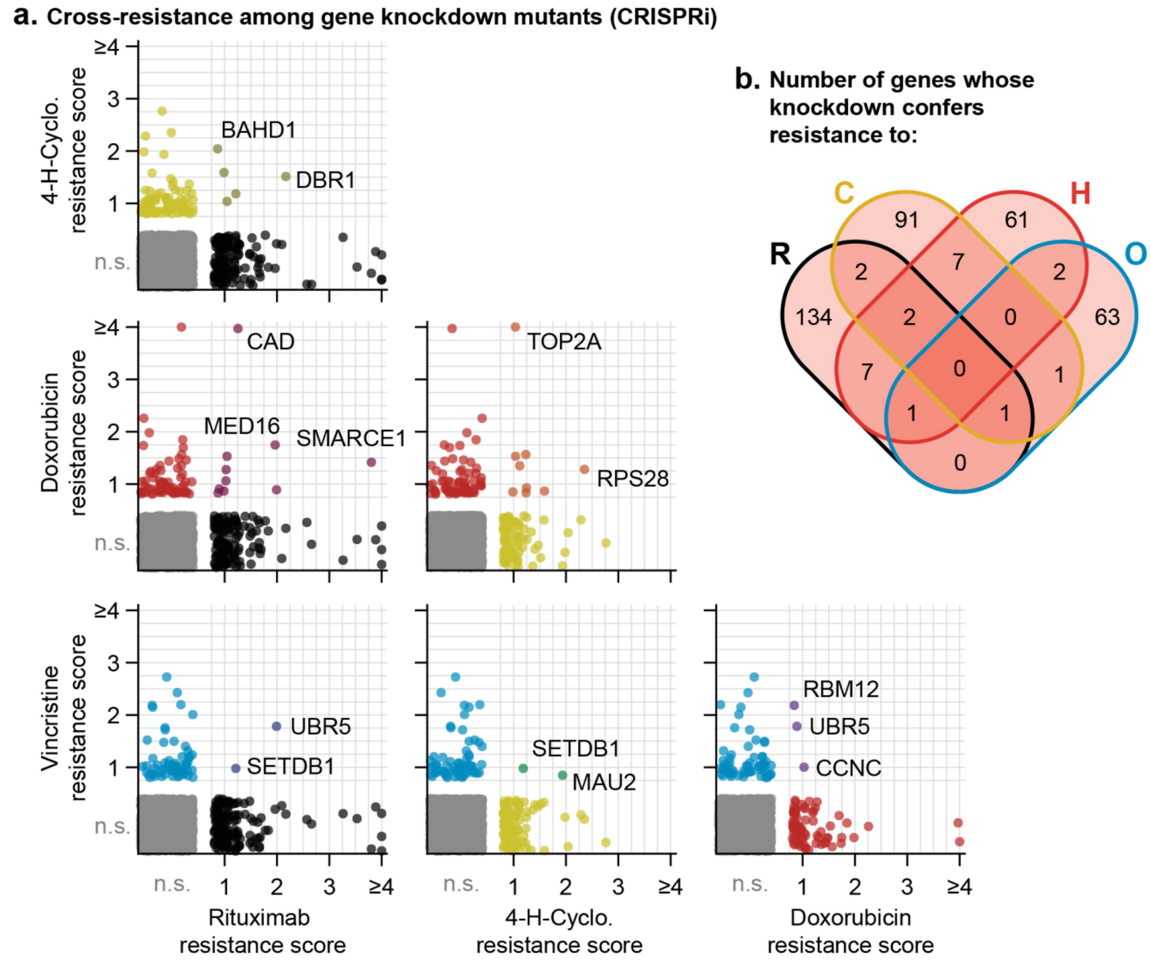

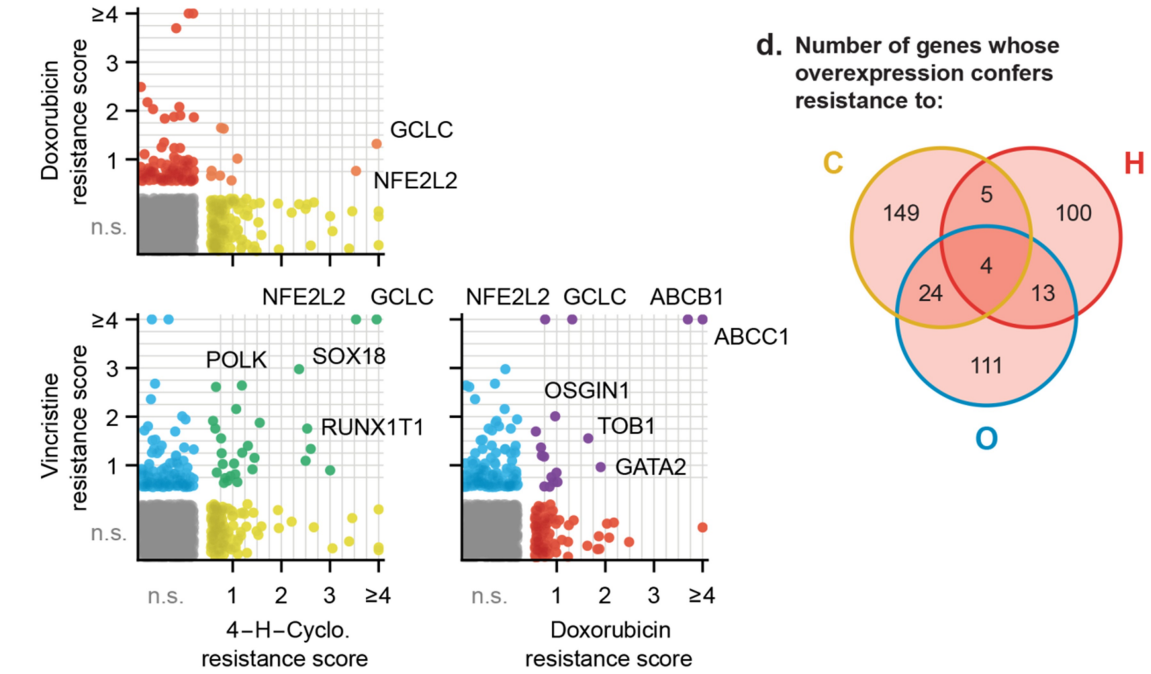

Figure 6. Cross-resistance analysis of the CRISPRi and CRISPRa screens reveals a small number of multi-drug resistance mechanisms. a. Scatter plots of resistance scores obtained in CRISPRi knockdown screens, for each pair of drugs in RCHO. Each dot represents a gene. Resistance scores were calculated from the product of the gene phenotype and the significance of the enrichment ($-\log_{10}P$). n.s., not significant; genes significant in one drug but not another are displayed against the left or bottom axis. Labeled genes are a partial list of top scoring hits. **b.** Venn diagram of genes whose knockdown by CRISPRi confers resistance to single or multiple drugs. **c.** Scatter plots of resistance scores obtained in the CRISPRa overexpression screens, for each pair of drugs in CHO. Data were analyzed and displayed as in (**a**). **d.** Venn diagram of genes whose overexpression by CRISPRa confers resistance to single or multiple drugs.

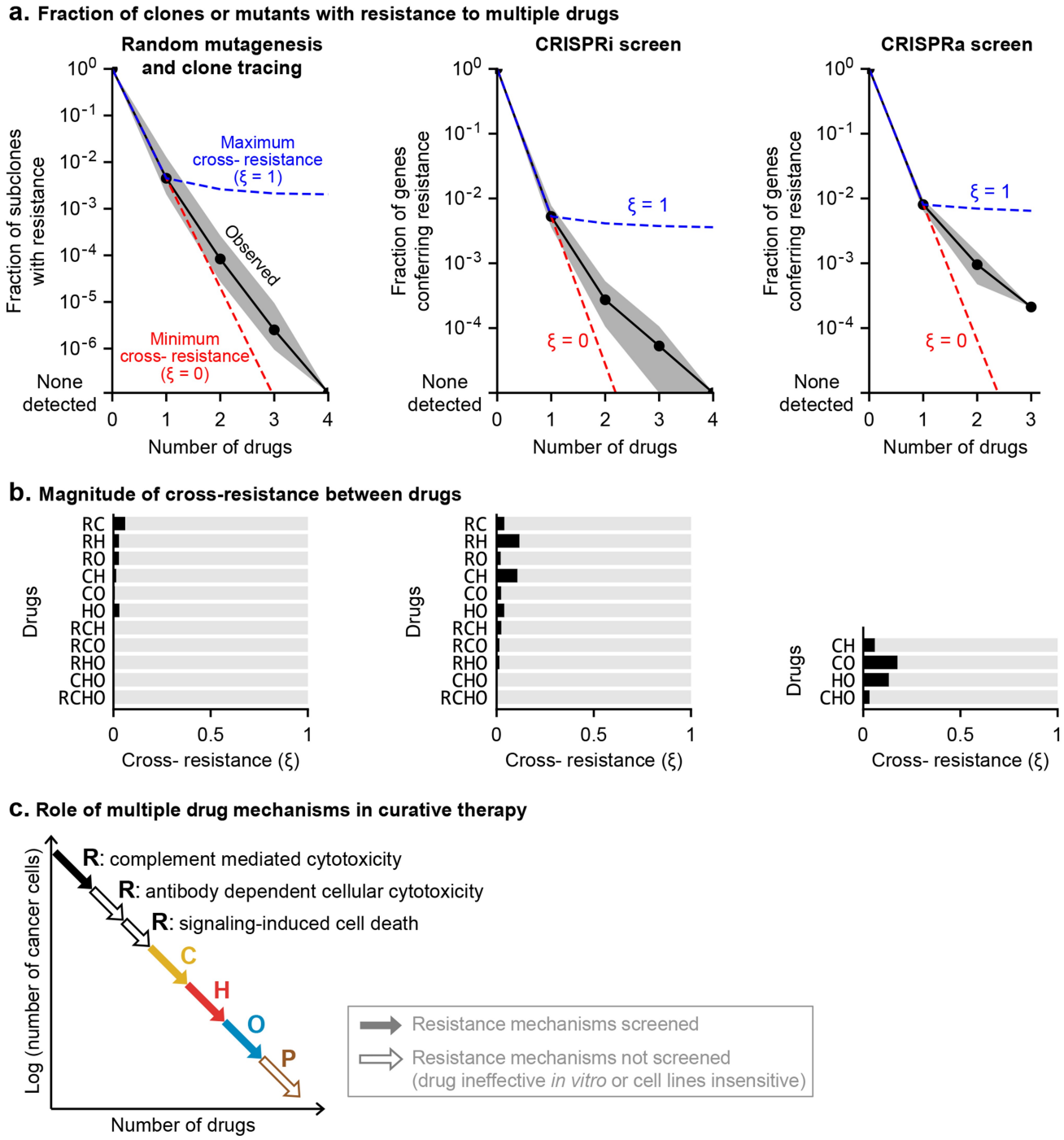

Figure 7. Cross-resistance between drugs in R-CHOP is close to its theoretical minimum. a. The fraction of clones, or gene perturbations by CRISPRi or CRISPRa, exhibiting resistance to one or more of the drugs in RCHO. Gray shading spans the range across different sets of drugs (e.g. 6 different pairs), and black points mark the average on a log scale. Dashed blue line: average frequency of Multi-Drug Resistance (MDR) if resistance is maximally overlapping (maximal overlap is the minimum of

constituent single drug MDR frequencies; cross resistance parameter $\xi = 1$). Dashed red line: average frequency of MDR if it is as rare as expected by statistically independent chances of resistance to each single drug (the product of single-drug MDR frequencies; $\xi = 0$). **b**. Strength of cross-resistance for different sets of drugs in RCHO**,** where ξ is calculated as a weighted sum of the maximum and minimum cross-resistance scenarios (for single-drug resistance rates 10^{-A} and 10^{-B}, MDR frequency = $\xi \times$ minimum(10^{-A} or 10^{-B}) + $(1 - \xi) \times 10^{-A-B}$). **c**. Conceptual schematic of the role of multiple drug mechanisms, each subject to different mechanisms of resistance, in the eradication of drug resistant clones and cure of a patient's cancer.

REFERENCES

1. Frei E, 3rd & Antman KH (2000) Principles of Dose, Schedule, and Combination Chemotherapy. *Holland-Frei Cancer Medicine*, eds Bast RC, Kufe DW, Pollock RE, Weichselbaum RR, Holland JF, & Frei E, 3rd (BC Decker, Hamilton (ON)), 5th edition. Ed.

2. Gaddum JH (1940) *Pharmacology* (Oxford University Press) 1st Ed.

3. Bliss CI (1939) The toxicity of poisons applied jointly. *Ann Appl Biol* 26(3):585-615.

4. Loewe S (1953) The problem of synergism and antagonism of combined drugs. *Arzneimittel-Forschung* 3(6):285-290.

5. Berenbaum MC (1989) What is synergy? *Pharmacological reviews* 41(2):93-141.

6. Law LW (1952) Effects of combinations of antileukemic agents on an acute lymphocytic leukemia of mice. *Cancer research* 12(12):871-878.

7. Law LW (1956) Differences between cancers in terms of evolution of drug resistance. *Cancer research* 16(7):698-716.

8. Frei E, 3rd*, et al.* (1965) The effectiveness of combinations of antileukemic agents in inducing and maintaining remission in children with acute leukemia. *Blood* 26(5):642-656.

9. Palmer AC & Sorger PK (2017) Combination Cancer Therapy Can Confer Benefit via Patient-to-Patient Variability without Drug Additivity or Synergy. *Cell* 171(7):1678-1691 e1613.

10. Greco WR, Bravo G, & Parsons JC (1995) The search for synergy: a critical review from a response surface perspective. *Pharmacological reviews* 47(2):331-385.

11. Bhang HE*, et al.* (2015) Studying clonal dynamics in response to cancer therapy using high-complexity barcoding. *Nature medicine* 21(5):440-448.

12. Johannessen CM*, et al.* (2013) A melanocyte lineage program confers resistance to MAP kinase pathway inhibition. *Nature* 504(7478):138-142.

13. Wang T, Wei JJ, Sabatini DM, & Lander ES (2014) Genetic screens in human cells using the CRISPR-Cas9 system. *Science* 343(6166):80-84.

14. Gilbert LA*, et al.* (2014) Genome-Scale CRISPR-Mediated Control of Gene Repression and Activation. *Cell* 159(3):647-661.

15. Shalem O*, et al.* (2014) Genome-scale CRISPR-Cas9 knockout screening in human cells. *Science* 343(6166):84-87.

16. le Sage C*, et al.* (2017) Dual direction CRISPR transcriptional regulation screening uncovers gene networks driving drug resistance. *Scientific reports* 7(1):17693.

17. Jost M*, et al.* (2017) Combined CRISPRi/a-Based Chemical Genetic Screens Reveal that Rigosertib Is a Microtubule-Destabilizing Agent. *Molecular cell* 68(1):210-223 e216.

18. Bester AC, *et al.* (2018) An Integrated Genome-wide CRISPRa Approach to Functionalize lncRNAs in Drug Resistance. *Cell* 173(3):649-664 e620.

19. Hata AN, *et al.* (2016) Tumor cells can follow distinct evolutionary paths to become resistant to epidermal growth factor receptor inhibition. *Nature medicine* 22(3):262-269.

20. Lakhtakia R & Burney I (2015) A Historical Tale of Two Lymphomas: Part II: Non-Hodgkin lymphoma. *Sultan Qaboos University medical journal* 15(3):e317-321.

21. Anonymous (2017) Rationalizing combination therapies. *Nature medicine* 23(10):1113.

22. Lehar J, *et al.* (2009) Synergistic drug combinations tend to improve therapeutically relevant selectivity. *Nature biotechnology* 27(7):659-666.

23. Alizadeh AA, *et al.* (2000) Distinct types of diffuse large B-cell lymphoma identified by gene expression profiling. *Nature* 403(6769):503-511.

24. Huang Y, *et al.* (2012) Outcome of R-CHOP or CHOP regimen for germinal center and nongerminal center subtypes of diffuse large B-cell lymphoma of Chinese patients. *TheScientificWorldJournal* 2012:897178.

25. Ludeman SM (1999) The chemistry of the metabolites of cyclophosphamide. *Current pharmaceutical design* 5(8):627-643.

26. Pickup ME (1979) Clinical pharmacokinetics of prednisone and prednisolone. *Clinical pharmacokinetics* 4(2):111-128.

27. Weiner GJ (2010) Rituximab: mechanism of action. *Seminars in hematology* 47(2):115-123.

28. Kobayashi H, Matsunaga Y, Uchiyama Y, Nagura K, & Komatsu Y (2013) Novel humanized anti-CD20 antibody BM-ca binds to a unique epitope and exerts stronger cellular activity than others. *Cancer medicine* 2(2):130-143.

29. Chakraborty J, Hayes M, English J, Baylis M, & Marks V (1981) Prednisolone concentrations in plasma, saliva and urine. *European journal of clinical pharmacology* 19(1):79-81.

30. Lamar Z (2016) The Role of Glucocorticoids in the Treatment of Non- Hodgkin Lymphoma. *Ann Hematol Oncol* 3(7).

31. Knutson SK, *et al.* (2014) Synergistic Anti-Tumor Activity of EZH2 Inhibitors and Glucocorticoid Receptor Agonists in Models of Germinal Center Non-Hodgkin Lymphomas. *PLoS One* 9(12):e111840.

32. Speth PA, van Hoesel QG, & Haanen C (1988) Clinical pharmacokinetics of doxorubicin. *Clinical pharmacokinetics* 15(1):15-31.

33. Gidding CE, Kellie SJ, Kamps WA, & de Graaf SS (1999) Vincristine revisited. *Critical reviews in oncology/hematology* 29(3):267-287.

34. de Jonge ME, Huitema AD, Rodenhuis S, & Beijnen JH (2005) Clinical pharmacokinetics of cyclophosphamide. *Clinical pharmacokinetics* 44(11):1135-1164.

35. Tran L, Baars JW, Aarden L, Beijnen JH, & Huitema AD (2010) Pharmacokinetics of rituximab in patients with CD20 positive B-cell malignancies. *Human antibodies* 19(1):7-13.

36. Hafner M, Niepel M, Chung M, & Sorger PK (2016) Growth rate inhibition metrics correct for confounders in measuring sensitivity to cancer drugs. *Nature methods* 13(6):521.

37. Goel S*, et al.* (2016) Overcoming Therapeutic Resistance in HER2-Positive Breast Cancers with CDK4/6 Inhibitors. *Cancer cell* 29(3):255-269.

38. Cutts JH (1961) The effect of vincaleukoblastine on dividing cells in vivo. *Cancer research* 21:168-172.

39. Barlogie B, Drewinko B, Johnston DA, & Freireich EJ (1976) The effect of adriamycin on the cell cycle traverse of a human lymphoid cell line. *Cancer research* 36(6):1975-1979.

40. Davidoff AN & Mendelow BV (1993) Cell-cycle disruptions and apoptosis induced by the cyclophosphamide derivative mafosfamide. *Experimental hematology* 21(7):922-927.

41. Odds FC (2003) Synergy, antagonism, and what the chequerboard puts between them. *The Journal of antimicrobial chemotherapy* 52(1):1.

42. Elion GB, Singer S, & Hitchings GH (1954) Antagonists of nucleic acid derivatives. VIII. Synergism in combinations of biochemically related antimetabolites. *The Journal of biological chemistry* 208(2):477-488.

43. Chou TC & Talalay P (1984) Quantitative analysis of dose-effect relationships: the combined effects of multiple drugs or enzyme inhibitors. *Advances in enzyme regulation* 22:27-55.

44. Cokol M, Kuru N, Bicak E, Larkins-Ford J, & Aldridge BB (2017) Efficient measurement and factorization of high-order drug interactions in Mycobacterium tuberculosis. *Science Advances* 3(10).

45. Pasqualucci L*, et al.* (2011) Analysis of the coding genome of diffuse large B-cell lymphoma. *Nature genetics* 43(9):830-837.

46. Sebastian E*, et al.* (2016) High-resolution copy number analysis of paired normal-tumor samples from diffuse large B cell lymphoma. *Annals of hematology* 95(2):253-262.

47. Chait R, Craney A, & Kishony R (2007) Antibiotic interactions that select against resistance. *Nature* 446(7136):668-671.

48. Sanger WG & Eisen JD (1976) Clastogenic effects of methylnitrosourea and ethylnitrosourea on chromosomes from human fibroblast cell lines. *Mutation research* 34(3):415-426.

49. Shibuya T & Morimoto K (1993) A review of the genotoxicity of 1-ethyl-1-nitrosourea. *Mutation research* 297(1):3-38.

50. Gilbert LA, *et al.* (2013) CRISPR-mediated modular RNA-guided regulation of transcription in eukaryotes. *Cell* 154(2):442-451.

51. Tanenbaum ME, Gilbert LA, Qi LS, Weissman JS, & Vale RD (2014) A protein-tagging system for signal amplification in gene expression and fluorescence imaging. *Cell* 159(3):635-646.

52. Li L, Wickham TJ, & Keegan AD (2001) Efficient transduction of murine B lymphocytes and B lymphoma lines by modified adenoviral vectors: enhancement via targeting to FcR and heparan-containing proteins. *Gene therapy* 8(12):938-945.

53. Horlbeck MA, *et al.* (2016) Compact and highly active next-generation libraries for CRISPR-mediated gene repression and activation. *eLife* 5:e19760.

54. Kampmann M, Bassik MC, & Weissman JS (2013) Integrated platform for genome-wide screening and construction of high-density genetic interaction maps in mammalian cells. *Proceedings of the National Academy of Sciences of the United States of America* 110(25):E2317-2326.

55. Thorn CF, *et al.* (2011) Doxorubicin pathways: pharmacodynamics and adverse effects. *Pharmacogenetics and genomics* 21(7):440-446.

56. Zoppoli G, *et al.* (2012) Putative DNA/RNA helicase Schlafen-11 (SLFN11) sensitizes cancer cells to DNA-damaging agents. *Proceedings of the National Academy of Sciences of the United States of America* 109(37):15030-15035.

57. Murai J, *et al.* (2018) SLFN11 Blocks Stressed Replication Forks Independently of ATR. *Molecular cell* 69(3):371-384 e376.

58. Cox PJ, Phillips BJ, & Thomas P (1975) The enzymatic basis of the selective action of cyclophosphamide. *Cancer research* 35(12):3755-3761.

59. Emadi A, Jones RJ, & Brodsky RA (2009) Cyclophosphamide and cancer: golden anniversary. *Nature reviews. Clinical oncology* 6(11):638-647.

60. Penning TM (2017) Aldo-Keto Reductase Regulation by the Nrf2 System: Implications for Stress Response, Chemotherapy Drug Resistance, and Carcinogenesis. *Chemical research in toxicology* 30(1):162-176.

61. Shain AH & Pollack JR (2013) The spectrum of SWI/SNF mutations, ubiquitous in human cancers. *PLoS One* 8(1):e55119.

62. Choi CH (2005) ABC transporters as multidrug resistance mechanisms and the development of chemosensitizers for their reversal. *Cancer cell international* 5:30.

63. Arnoldo A, *et al.* (2014) A genome scale overexpression screen to reveal drug activity in human cells. *Genome medicine* 6(4):32.

64. Zanotto-Filho A, *et al.* (2016) Alkylating Agent-Induced NRF2 Blocks Endoplasmic Reticulum Stress-Mediated Apoptosis via Control of Glutathione Pools and Protein Thiol Homeostasis. *Molecular cancer therapeutics* 15(12):3000-3014.

65. Kitamura H & Motohashi H (2018) NRF2 addiction in cancer cells. *Cancer science* 109(4):900-911.

66. Bansal A & Simon MC (2018) Glutathione metabolism in cancer progression and treatment resistance. *The Journal of cell biology* 217(7):2291-2298.

67. Andreadis C*, et al.* (2007) Members of the glutathione and ABC-transporter families are associated with clinical outcome in patients with diffuse large B-cell lymphoma. *Blood* 109(8):3409-3416.

68. Michel JB, Yeh PJ, Chait R, Moellering RC, Jr., & Kishony R (2008) Drug interactions modulate the potential for evolution of resistance. *Proceedings of the National Academy of Sciences of the United States of America* 105(39):14918-14923.

69. Lossos IS*, et al.* (2004) Prediction of survival in diffuse large-B-cell lymphoma based on the expression of six genes. *The New England journal of medicine* 350(18):1828-1837.

70. Natkunam Y*, et al.* (2008) LMO2 protein expression predicts survival in patients with diffuse large B-cell lymphoma treated with anthracycline-based chemotherapy with and without rituximab. *Journal of clinical oncology : official journal of the American Society of Clinical Oncology* 26(3):447-454.

71. Roberts AM, Ward CC, & Nomura DK (2017) Activity-based protein profiling for mapping and pharmacologically interrogating proteome-wide ligandable hotspots. *Current opinion in biotechnology* 43:25-33.

72. Moret N*, et al.* (2018) Cheminformatics tools for analyzing and designing optimized small molecule libraries. *bioRxiv*.

73. Yeh PJ, Hegreness MJ, Aiden AP, & Kishony R (2009) Drug interactions and the evolution of antibiotic resistance. *Nature reviews. Microbiology* 7(6):460-466.

74. Reff ME*, et al.* (1994) Depletion of B cells in vivo by a chimeric mouse human monoclonal antibody to CD20. *Blood* 83(2):435-445.

75. Dall'Ozzo S*, et al.* (2004) Rituximab-dependent cytotoxicity by natural killer cells: influence of FCGR3A polymorphism on the concentration-effect relationship. *Cancer research* 64(13):4664-4669.

76. Dotan E, Aggarwal C, & Smith MR (2010) Impact of Rituximab (Rituxan) on the Treatment of B-Cell Non-Hodgkin's Lymphoma. *P & T : a peer-reviewed journal for formulary management* 35(3):148-157.

77. Chou TC (2010) Drug combination studies and their synergy quantification using the Chou-Talalay method. *Cancer research* 70(2):440-446.

78. Al-Lazikani B, Banerji U, & Workman P (2012) Combinatorial drug therapy for cancer in the post-genomic era. *Nature biotechnology* 30(7):679-692.

79. Sun X, Vilar S, & Tatonetti NP (2013) High-throughput methods for combinatorial drug discovery. *Science translational medicine* 5(205):205rv201.

80. Neal AJ & Hoskin PJ (2009) *Clinical oncology : basic principles and practice* (Hodder Arnold, London) 4th Ed pp xiv, 402 p.

81. Law LW (1952) Origin of the resistance of leukaemic cells to folic acid antagonists. *Nature* 169(4302):628-629.

82. Schnipper L (1986) Clinical implications of tumor-cell heterogeneity. *The New England journal of medicine* 314(22):1423-1431.

83. Bozic I*, et al.* (2013) Evolutionary dynamics of cancer in response to targeted combination therapy. *eLife* 2:e00747.

84. Han K*, et al.* (2017) Synergistic drug combinations for cancer identified in a CRISPR screen for pairwise genetic interactions. *Nature biotechnology* 35(5):463-474.

85. Martin M (2011) Cutadapt removes adapter sequences from high-throughput sequencing reads. *2011* 17(1):3.

86. Eden E, Navon R, Steinfeld I, Lipson D, & Yakhini Z (2009) GOrilla: a tool for discovery and visualization of enriched GO terms in ranked gene lists. *BMC bioinformatics* 10:48.